


 Cite this: *Phys. Chem. Chem. Phys.*,  
 2024, 26, 24261

# Shortwave infrared polymethine dyes for bioimaging: ultrafast relaxation dynamics and excited-state decay pathways†

 Laura M. Obloy, , Steffen Jockusch  and Alexander N. Tarnovsky \*

Excited-state relaxation in two prototypical shortwave infrared (SWIR) polymethine dyes developed for bioimaging, heptamethine chromenylum Chrom7 and flavylum Flav7, is studied by means of femtosecond transient absorption with broadband ultraviolet-to-SWIR probing complemented by steady-state and time-resolved fluorescence and phosphorescence measurements. The relaxation processes of the dyes in dichloromethane are resolved with sub-100 fs temporal resolution using SWIR, near-IR, and visible photoexcitation. Different population members of the ground-state inhomogeneous ensemble are found to equilibrate *via* skeletal deformation changes with time constants of 90 fs and either 230 fs (Chrom7) and 350 fs (Flav7) followed by slower evolution matching the 1-ps timescale of diffusive solvation dynamics. Molecules excited into high-lying singlet electronic states ( $S_n$ ) by visible excitation repopulate with time constants of 400 fs (Chrom7) and 450 fs (Flav7) the corresponding first excited singlet  $S_1$  states, which decay within several hundreds of picoseconds in dichloromethane and chloroform solvents. Vibrational relaxation in  $S_1$  for both Chrom7 and Flav7 in dichloromethane occurs with time constants of 350 and 800 fs for excess of vibrational energy of  $\sim 1000$  and  $10\,000\text{ cm}^{-1}$  deposited by near-IR and visible excitation, respectively. Two competing non-radiative processes are present in  $S_1$ : temperature-independent internal conversion, and thermally-activated twisting about a carbon-carbon bond of the conjugated chain, which is substantial at room temperature but essentially nonreactive, producing traces of isomer product. Intersystem crossing in  $S_1$ , and thus the triplet quantum yield, is minor. The importance of absorption bands from the excited  $S_1$  state in applications requiring high-intensity excitation conditions is discussed.

 Received 5th April 2024,  
 Accepted 23rd May 2024

DOI: 10.1039/d4cp01411a

rsc.li/pccp

## Introduction

The development of shortwave infrared (SWIR) emitters for bioimaging applications is of significant interest.<sup>1–5</sup> The SWIR portion of the electromagnetic spectrum extends from about 900 to 2500 nm. Compared with *in vivo* imaging applications in the near-IR range, SWIR imaging presents several substantial advantages<sup>6</sup> such as less autofluorescence and scattering produced by the tissue as well as a larger penetration depth into the tissue opening an opportunity for deep tissue imaging. Organic fluorophores exhibit low toxicity and are removed from the body by well-understood mechanisms. Also, they can target specific biomolecules either inherently or by design. These favorable traits make organic fluorophores to be the aspiring and most common imaging agents and fluorescent labels.<sup>2,7–10</sup> To improve the efficiency of SWIR fluorophores for bioimaging

applications, a comprehensive understanding of the excited-state radiationless relaxation pathways competing with fluorescence in these molecular systems should be gained. This should permit identifying key drawbacks in the fluorophores design and lead to further development of bright and stable organic SWIR emitters with enhanced, tailored photodynamics.

Dyes of the polymethine group are one of the most widely used fluorescent agents.<sup>7–12</sup> Their ubiquitous use in photographic, laser, and photonic industries was reviewed.<sup>9,13–15</sup> In biophysical and biomedical applications, because of photostability as well as intense absorption and fluorescence, the indocarbocyanines, especially Cy3, Cy5, and Cy7 of the Cy series<sup>16–22</sup> have become broadly used. They consist of two indolenine heterocyclic end rings connected by 3, 5, or 7  $-\text{CH}=\text{methine}$  units forming the  $\pi$ -conjugated chain. In polymethines, the main absorption band is due to a dipole-allowed  $\pi\pi^*$  transition between the ground  $S_0$  and lowest excited singlet  $S_1$  states in the most thermodynamically stable planar *trans*-isomer (sterically non-hindered dyes<sup>23</sup>). An extra  $-\text{CH}=\text{CH}-$  unit in the conjugation chain produces an approximately 100-nm displacement of the  $S_0-S_1$  band towards longer wavelengths

Department of Chemistry and the Center for Photochemical Sciences, Bowling Green State University, Bowling Green, OH 43403, USA. E-mail: atarnov@bgsu.edu

† Electronic supplementary information (ESI) available. See DOI: <https://doi.org/10.1039/d4cp01411a>



Scheme 1 Structures of the studied dyes (counterion,  $\text{BF}_4^-$ ).

known as a vinylenic shift. Although the absorption of Cy7-like heptamethine dyes reaches the 800-nm range, it does not extend further than  $\sim 850$  nm. Further lengthening of the polymethine chain is possible,<sup>3,12</sup> but it may enhance the likelihood of thermal instability and photodecomposition, thus hampering the biological imaging applications.<sup>24</sup> Extending heterocyclic conjugation, rather than elongating the polymethine chain, is a viable alternative. A recently developed flavylium polymethine dye, Flav7 in Scheme 1,<sup>24,25</sup> possesses two dimethyl-flavylium heterocyclic end groups in place of the indolenines in the Cy7-like dyes producing, in comparison, a  $\sim 200$ -nm shift of absorption and fluorescence spectra into the IR region.

Efficient SWIR fluorescence is critical for bioimaging; however, SWIR fluorophores exhibit low emission quantum yields and it is

not clear if other reasons, apart from a small  $S_0$ - $S_1$  energy gap, affect the  $S_1$  deactivation. Flav7 was the brightest organic SWIR emitter at the time of publication<sup>24,25</sup> and remains one of the brightest at present. Generally, for polymethines, in agreement with Kasha's rule<sup>26</sup>  $S_n$  are much less emissive than  $S_1$  states, which in the absence of intermolecular relaxation, decay *via* competing radiative and non-radiative processes of internal conversion (IC), photoisomerization, and intersystem crossing (ISC), Fig. 1a. Photoisomerization, which is temperature and viscosity dependent, is predominant in short-chain and pentamethine cyanines in room-temperature fluid solutions,<sup>27-31</sup> but becomes less dominant in heptamethines under the same conditions.<sup>32-34</sup> Whereas the geometry restriction imparted at the central region of the heptamethine chain moderately affects the photoisomerization,<sup>35-37</sup> conformational restraint imparted along the entire chain is reported to stop the photoisomerization entirely.<sup>22</sup> For unrestrained dyes, the Rullière model has been widely invoked in which the  $S_1$  *trans*-isomer overcomes the photoisomerization barrier (rate constant,  $k_{\text{ph}}$ ) to yield the  $90^\circ$ -twisted structure, which either yields the  $S_0$  *cis*-photoisomer or returns to the parent  $S_0$  *trans*-form with  $\phi$  and  $1 - \phi$  branching ratio.<sup>27-29</sup> Advanced quantum chemistry computations on streptocyanines<sup>38,39</sup> suggest that the initial in-plane symmetric stretching in the Franck-Condon (FC) region on the  $S_1$  potential energy surface (PES) is followed by torsional motion dominated by twisting about one of the central carbon-carbon conjugated bonds at the end. This takes the molecule to an extended  $S_1 \rightarrow S_0$  conical intersection (CI) seam located close to the  $90^\circ$ -twisted state, but on the *trans*-side. The recovery of the  $S_0$  *trans*-form is thus favored, which is consistent with  $<10\%$  quantum yields of the photoisomer formation in sterically non-hindered penta- and heptamethines.<sup>30-32,40</sup> Because of large  $k_{\text{ph}}$  of

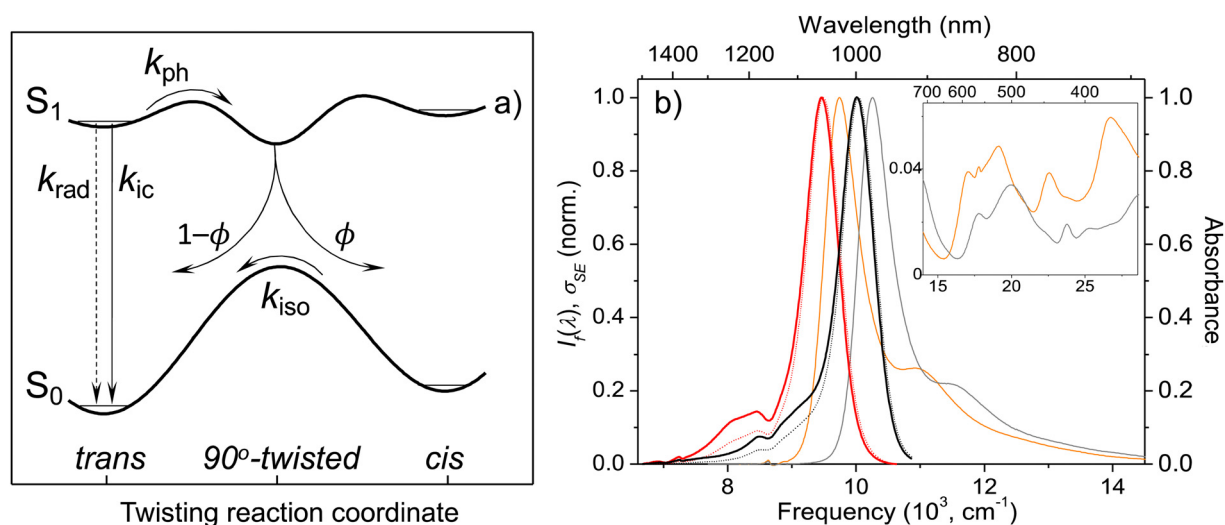


Fig. 1 Model potential energy diagram<sup>27</sup> used in literature to interpret the photophysics and photochemistry of polymethine dyes. (a) a thermodynamically stable *trans*-form excited into  $S_1$  undergoes radiative decay, direct internal conversion, and thermally activated crossing over the photoisomerization barrier along the twisting reaction coordinate. The corresponding rate constants are  $k_{\text{rad}}$ ,  $k_{\text{ic}}$ , and  $k_{\text{ph}}$ . From the  $90^\circ$  twisted  $S_1$ -state, the molecule branches either into the *trans*- or *cis*- $S_0$  forms. The ground-state isomerization rate constant for reformation of the *trans*-isomer is  $k_{\text{iso}}$ . Normalized steady-state absorption (orange and grey) and fluorescence<sup>25</sup> spectra ( $I_f(\lambda)$ , red and black dotted curves) of Flav7 and Chrom7 in anhydrous  $\text{CH}_2\text{Cl}_2$ , and the constructed  $\sigma_{\text{SE}}(\lambda)$  stimulated emission cross-section spectra (solid red and black curves), (b) the inset shows the short-wavelength absorbance of Flav7 and Chrom7 measured in solutions of larger overall absorbance and appropriately scaled to match the spectra in the main panel.

these and shorter-chain dyes in fluid solutions, unless ISC is aided by heavy atom substituents, the quantum yield of the formation of the lowest excited triplet  $T_1$  state ( $\Phi_{isc}$ ) is small. The  $\Phi_{isc}$  values of  $\sim 0.001$ <sup>30,31,33,41–45</sup> are typical; however, 0.03<sup>16,17</sup> was recently proposed for Cy3 and Cy5. The twisting pathway leading to the  $S_0$  *trans*-form (*i.e.*, unreactive) is thermally-activated and controlled by the photoisomerization barrier and, therefore, should be distinguished from 'direct'  $S_1 \rightarrow S_0$  IC within the planar *trans*-form (rate constant,  $k_{ic}$ ). Direct IC is very weakly viscosity and temperature dependent occurring even at low temperatures and/or in highly viscous solutions,<sup>29,33,44,46–48</sup> and therefore, does not involve a large structural change. The underlying theory for direct IC is the energy gap law,<sup>49</sup> according to which the energy decays intramolecularly from the donor excited electronic state to the high-frequency-mode vibrational states of the acceptor electronic state. When the displacement between the involved PESs is not large, the decay rate constant is predicted to increase exponentially with decreasing energy separation between the electronic states. This behavior was found in several organic systems such as aromatic hydrocarbons,<sup>50</sup> linear polyenes, and carotenoids.<sup>51–53</sup> However, the exact nature of the accepting modes is still under debate with C=C,<sup>52,54–57</sup> C–H,<sup>57–59</sup> and organic alkenyl C–H<sup>22,60</sup> stretching as well as N–H and O–H vibrations<sup>61</sup> all having been proposed. Vibrational overlap between the narrowly separated  $S_1$  and  $S_0$  states becomes substantial and is considered in literature to be the reason for short  $S_1$ -state lifetimes and low quantum yields of SWIR fluorophores.

The main objective of this work is to characterize excited-state relaxation processes following photoexcitation of two SWIR polymethine dyes, Flav7 and closely related Chrom7, where in the latter the phenyl groups are replaced by *tert*-butyl groups. Experimental work on the excited-state relaxation pathways of SWIR dyes is limited, and further studies on these two systems should lead to a deeper understanding of photophysics and photochemistry of SWIR fluorophores in general. We have used femtosecond transient absorption spectroscopy to capture the evolution of the photoinduced reaction starting from the very initial events. Flav7 and Chrom7 were excited in the (i) low-energy wing of the  $S_0$ – $S_1$  absorption band, 1042 and 990 nm, respectively, (ii) shoulder of the  $S_0$ – $S_1$  band, namely 925 nm, and (iii) 500-nm region of the congested  $S_0$ – $S_n$  absorption bands where the photostability of these dyes was previously evaluated.<sup>24,25</sup> In addition, we have performed a series of femtosecond and nanosecond transient absorption as well as steady-state and time-resolved emission measurements at different temperatures to obtain the hitherto unknown information regarding the involvement of photoisomerization in the  $S_1$  relaxation and the energetics of the  $T_1$  state.

## Results and discussion

### Steady-state absorption and emission: construction of cross-section spectra

The X-ray crystal structure of Chrom7 and JuloFlav5 closely related to Flav7 is all-*trans*,<sup>25</sup> which implies the same conformation in solution based on the literature.<sup>23</sup> The UV-vis

absorption spectra of Chrom7 and Flav7 in  $CH_2Cl_2$  exhibit intense bands peaking at 975 and 1027 nm due to the  $S_0$ – $S_1$  transition, Fig. 1b. The shoulders at shorter wavelengths ( $\sim 880$  nm in Chrom7 and 915 nm in Flav7) shifted by  $\sim 1230$   $cm^{-1}$  from the  $S_0$ – $S_1$  band maxima are assigned to the 0-1' vibronic bands,<sup>62</sup> where 0 are 1' label the optically active vibrational states in  $S_0$  and  $S_1$ , respectively. The frequency at which the approximately mirror-symmetrical fluorescence<sup>25</sup> and absorption spectra overlap can serve as an estimate for the  $S_0$ – $S_1$  energy gap; it is 10 140  $cm^{-1}$  for Chrom7 and 9700  $cm^{-1}$  for Flav7. The analysis of transient absorption spectra requires the knowledge of  $S_0$ – $S_1$  absorption ( $\sigma_A$ ) and  $S_1$ – $S_0$  stimulated emission ( $\sigma_{SE}$ ) cross-section spectra. The  $\sigma_A$  spectrum is given as:  $\sigma_A(\lambda) = \varepsilon(\lambda) \times 2303/N_A$ , where  $N_A$  is the Avogadro number and  $\varepsilon(\lambda)$  is the extinction coefficient spectrum. Based on the maximum  $\varepsilon$  values (Table 1), the maximum  $\sigma_A$  values are calculated to be  $9.57 \times 10^{-16}$  and  $9.22 \times 10^{-16}$   $cm^2$  for Chrom7 and Flav7, respectively. The  $\sigma_{SE}(\lambda)$  spectra are obtained from the fluorescence spectra when applying necessary scaling corrections for the frequency of the emitted light,<sup>63</sup> as detailed in the ESI,<sup>†</sup> section, and further assuming that the  $S_0$ – $S_1$  and  $S_1$ – $S_0$  transition dipole moments are the same.<sup>64</sup> The resulting spectra (Fig. 1b) exhibit the  $\sigma_{SE}(\lambda)$  maximum of  $1.09 \times 10^{-15}$  and  $1.14 \times 10^{-15}$   $cm^2$  for Chrom7 and Flav7, respectively.

### Radiative and total lifetime of the $S_1$ state

The dye  $S_1$  lifetime can be calculated using the formula  $\tau_f^{calc} = \Phi_f/k_{rad}$  from the known fluorescence quantum yield  $\Phi_f$  and the radiative rate constant  $k_{rad}$ , which in its turn can be calculated using the Strickler-Berg equation:<sup>65</sup>  $k_{rad} = 2.88 \times 10^{-9} n_f^2 \int_{\bar{\nu}} \varepsilon(\bar{\nu}) d \ln \bar{\nu} \int_{\bar{\nu}_f} I_f(\bar{\nu}) d\bar{\nu} / \int_{\bar{\nu}_f} I_f(\bar{\nu}) \bar{\nu}^{-3} d\bar{\nu}$ . In the equation,  $\varepsilon(\bar{\nu})$  is the  $S_0 \rightarrow S_1$  extinction coefficient spectrum,  $I_f(\bar{\nu})$  is the  $S_1 \rightarrow S_0$  fluorescence spectrum,  $\bar{\nu}$  is the frequency (expressed in wavenumber units), and  $n_f$  is the mean refractive index of the solvent over the fluorescence spectrum. The refractive index of  $CH_2Cl_2$  in the 1- $\mu m$  region is about 1.422.<sup>66,67</sup> The  $\int_{\bar{\nu}} \varepsilon(\bar{\nu}) d \ln \bar{\nu}$  integrals for Flav7 and Chrom7 were evaluated for  $\bar{\nu} \leq 15 100$   $cm^{-1}$  to account only for the  $S_0 \rightarrow S_1$  transition in question, yielding  $k_{rad}$  of  $1.241 \times 10^8$  and  $1.356 \times 10^8$   $s^{-1}$ , respectively, Table 1.

### Excitation into the low-energy part of the absorption spectrum

Chrom7 was excited at 990 nm and Flav7 at 1042 nm at the low-energy wing of their  $S_0 \rightarrow S_1$  0-0' vibronic transition to

Table 1 Summary of calculated and measured  $S_1$  lifetimes of Chrom7 and Flav7 in dichloromethane<sup>a–e</sup> and chloroform<sup>f,g</sup>

Dye	$\varepsilon$ ( $M^{-1} cm^{-1}$ )	$\Phi_f$ (%)	$k_{rad}$ , $10^8$ ( $s^{-1}$ )	$\tau_f^{calc}$ (ps)	$\tau_f^{exp}$ (ps)	
					TCSPC <sup>b</sup>	This work
Chrom7	250 250 252 000 <sup>a</sup>	1.7 <sup>a</sup>	1.356	125 148	162 <sup>c</sup> , 158 <sup>d</sup> , 210 <sup>f</sup>	
Flav7	241 000 <sup>a</sup>	0.61 <sup>a</sup>	1.241	49 68	69 <sup>e</sup> , 67 <sup>d</sup> , 77 <sup>g</sup>	

<sup>a</sup> Ref. 24. <sup>b</sup> After deconvolution with IRF.<sup>25</sup> <sup>c</sup> Determined from  $S_1$  ESA decay. Excitation (nm): <sup>c</sup> 990, <sup>d</sup> 925, <sup>e</sup> 1042, <sup>f</sup> 990, <sup>g</sup> 1042, all this work.

minimize contribution from vibrational relaxation to the dynamics. In transient absorption spectra, Fig. 2, the prominent negative  $\Delta A$  signals are observed at probe wavelengths longer than  $\sim 800$ -nm. They represent excitation-induced probe gain due to ground-state bleach (GSB) and stimulated emission (SE) caused by the depletion of the  $S_0$  population and the population of the  $S_1$  state. The positive  $\Delta A$  signals represent induced absorption (*i.e.*, probe loss) and emerge as a  $\sim 420$ – $780$  nm broad band with two maxima, 612 and 657 nm for Chrom7 and 622 and 685 nm for Flav7. They decay concurrently to SE signals and, therefore, are assigned to excited-state absorption (ESA) from  $S_1$  to higher  $S_n$  states.

The overall photoinduced dynamics can be divided into three different stages. As soon as the 90-fs excitation and probe pulses begin to temporally overlap (delay time,  $-200$  fs), spectrally narrow positive (in the  $\sim 625$  nm region) and negative (in the vicinity of the excitation wavelength)  $\Delta A$  signals are observed for Chrom7 and Flav7, Fig. 3. The initial negative signals broaden and shift to shorter wavelengths as delay times progress to 250 fs. The initial positive signals broaden faster, *i.e.*, within the first 200 fs, while shifting to longer wavelengths. These sharp short-time  $\Delta A$  signals are characteristic to hole burning dynamics.<sup>68–71</sup> From 250 fs to 2 ps, the  $\Delta A$  spectra undergo only a modest reshaping. Afterwards, the amplitude of  $\Delta A$  signals decays uniformly and single-exponentially,

suggesting that the relaxation is now exclusively determined by the  $S_1$  lifetime. The  $S_1$  lifetime found for Flav7 is the same as the one reported in time-correlated single photon counting (TCSPC) experiments ( $68$  ps<sup>25</sup>), whereas the  $S_1$  lifetime of 162 ps for Chrom7 is somewhat longer (TCSPC,  $148$  ps<sup>25</sup>), Table 1. Confirming the  $S_1$  lifetimes using the superior temporal resolution was desirable as it is known that TCSPC may not be accurate enough to measure tens of picoseconds lifetimes of the same temporal duration as the instrument response function (IRF) of the technique.

When the  $S_1$  decay is complete, very weak  $\Delta A$  signals persisting to the longest investigated 2-ns delay time were observed: induced absorption from 1020 to 1120 nm for Flav7, and induced absorption in the 1020–1070 and 600-nm regions and bleach between 970 and 1020 nm for Chrom7, Fig. S1 (ESI<sup>†</sup>). Thermal heating and photodegradation can be ruled out as possible reasons for these signals because the excitation energy used was well below  $100$  nJ pulse<sup>-1</sup> and the UV-vis spectra of the solutions measured before and after the experiments showed no changes. *Trans-cis* photoisomerization or ISC in the *trans*  $S_1$ -state yield a long-lived product, the  $S_0$  *cis*-isomer or the *trans*-form in the  $T_1$  state, also causing GSB of the parent *trans*-form. We investigated the transient absorption of Chrom7 solutions saturated with  $O_2$  after a nanosecond pulsed 532-nm excitation, Fig. S2 (ESI<sup>†</sup>).  $O_2$  is known to act as a triplet state



Fig. 2 Short- (a) and (d), intermediate- (b) and (e), and long- (c) and (f) time  $\Delta A$  spectra of 990-nm excited Chrom7 (a)–(c) and 1042-nm excited Flav7 (d)–(f): delay times between excitation and probe pulses expressed in picoseconds are given inside each panel.



**Fig. 3** Short-time behavior of  $\Delta A$  kinetic traces at representative probe wavelengths within  $S_0$ – $S_1$  absorption and stimulated emission regions for Chrom7 excited at 990 nm, (a) and Flav7 excited at 1042 nm, (b). The kinetic traces are normalized to the maximum short-time negative  $\Delta A$  signal. Insets: The same  $\Delta A$  data to 2 ns before normalization. Note the decadic logarithmic time scale after 10 ps. The bell-like curve is the excitation-probe cross-correlation function (CCF, 158 fs fwhm).

quencher.<sup>72</sup> If  $T_1 \rightarrow T_n$  absorption were responsible for the observed transient absorption, the  $\Delta A$  signal should have decayed within the investigated 4  $\mu$ s window in the  $O_2$ -saturated solution compared to the solution in the equilibrium with air at 1 atm ( $O_2$  equilibrium concentration in  $CH_2Cl_2$ : 2.2 mmol liter<sup>-1</sup><sup>73</sup>). Because this was not observed, Fig. S2 (ESI<sup>†</sup>), we concluded the long-time  $\Delta A$  signals in the femtosecond experiments are due to the isomer product. The photoisomer absorption in penta- and heptamethine dyes is typically red-shifted with respect to that of the parent *trans*-form,<sup>30,31,33,74–76</sup> consistent with our assignment. The photoisomer quantum yield of  $1.8 \times 10^{-3}$  and  $6.4 \times 10^{-3}$  for Chrom7 and Flav7, respectively, can be estimated under the assumption that the maximum extinction coefficients for *trans* and photoisomer forms are similar,<sup>30,31,33,74–76</sup> and using the ratio of the 1–2 ns  $\Delta A$  signals ( $<0.04$  mOD and  $<0.07$  mOD, Fig. S1, ESI<sup>†</sup>) to the GSB maximum taken to be a half (to exclude the SE contribution) of the maximum negative  $\Delta A$  signal,  $-0.042$  and  $-0.023$  (Fig. 2) at 300 fs after completion of fast hole-burning dynamics.

Ultrafast transient absorption experiments were also performed for both dyes in  $CHCl_3$  to compare and determine the  $S_1$  lifetimes. The fits of the  $\Delta A$  kinetic traces acquired within the region of ESA from the  $S_1$  state, Fig. S3 (ESI<sup>†</sup>), yielded the lifetime of  $210 \pm 3$  ps for Chrom7 and  $77 \pm 2$  ps for Flav7 (22 °C, Table 1).

### Ultrafast transient absorption: 925-nm excitation into the vibronic shoulder

In response to the abrupt solute charge redistribution caused by excitation, various re-equilibration processes occur on ultrafast timescales to a varying degree such as solvation dynamics and solute vibrational relaxation. Rearrangement of the nearby solvent to accommodate the new solute charge distribution may initially occur as fast as 20–60 fs depending on solvent, and typically lasts about a few picoseconds. Vibrational energy redistribution in the polyatomic solutes may be as fast as 30–100 fs<sup>71,77–79</sup> to several hundreds of femtoseconds, and is

followed by picosecond energy transfer to the surrounding solvent.<sup>80–82</sup> To gauge the contribution of these processes into the initial dynamics, we utilized 925-nm excitation into the 0-1' vibronic shoulder and probed the  $S_1$  ESA region, Fig. 4. This excitation produces the excess vibrational energy of 700  $cm^{-1}$  for Chrom7 and 1200  $cm^{-1}$  for Flav7 in their  $S_1$  states with respect to the red-wing excitation. The  $\Delta A$  spectra of both dyes excited at 925-nm initially ( $-200$  fs) exhibit sharp ESA features, which broaden on their red side as the excitation and probe pulses better temporally overlap. At 100 fs, the ESA spectra already look like those in Fig. 3, displaying the 612-nm (Chrom7) and 622 nm (Flav7) bands, but the weaker bands at 657 nm (Chrom7) and 685 nm (Flav7) fully develop at  $\sim 1$ –2 ps *via* red-side broadening and blue-side narrowing, Fig. S4 (ESI<sup>†</sup>). Afterwards, the  $\Delta A$  spectra remained unaltered in shape and decayed single-exponentially with the  $S_1$  lifetimes, Table 1.

### Hole burning

The spectrally sharp features in short-time  $\Delta A$  spectra (Fig. 2) are due to hole burning and hole replica. If the transition energies of solute molecules are inhomogeneously distributed, only a fraction of these molecules whose transition energies are equal to the excitation photon energy, will be photoexcited.<sup>83</sup> As a result, a population hole is burned in the thermally-equilibrated ground-state solute-solvent configurational distribution and can be seen as the series of narrow vibronic lines missing from the initial solute absorption or, specifically in transient absorption experiments, as the series of spectrally narrow GSB signals. The population excited into the FC state initially represents the replica of the ground-state hole: a narrow ensemble localized on the multidimensional solute-solvent PES of the excited state. The hole replica is seen through spectrally narrow negative (SE) and positive (ESA)  $\Delta A$  signals. Thus, the short- and long-wavelength sides of the initial, negative sharp feature at 990 nm in Chrom7 and 1042 nm in Flav7 (Fig. 2) are due to the  $S_0$  absorption hole and the  $S_1$  stimulated emission hole replica. These  $\Delta A$  features



Fig. 4 Transient absorption spectra of Chrom7 (a)–(c) and Flav7 (d)–(f) in  $\text{CH}_2\text{Cl}_2$  at short (a) and (d), intermediate (b) and (e), and long (c) and (f) times following 90-fs 925-nm excitation. Delay times between the excitation and probe pulses are given in the legends. The representative  $\Delta A$  kinetic traces at several probe wavelengths and the fits with CCF deconvolution are shown for Chrom7 in (g) and Flav7 in (h). Note the decadic logarithmic time scale after 10 ps.

rapidly broaden on the high-energy side from 990 to 980 nm in Chrom7 and 1023 to 1015 nm in Flav7 between  $-100$  and 100 fs. Analogous dynamics was observed previously in several dyes.<sup>84,85</sup> When excitation is at the low-energy side of absorption spectrum,<sup>84–86</sup> as the re-equilibration begins on the  $S_0$  solute–solvent configurational potential the GSB develops on the high-energy side of the initial hole. At the same time, the hole replica is positioned in the minimum of the solute–solvent configurational potential and, consequently, hole replica SE does not show time-dependent shift, Fig. 5a. Hole replica ESA is also stationary. The shift of the positive  $\Delta A$  maxima from 621 to 623 nm for Chrom7 and 608 to 612 nm for Flav7 between  $-100$  and 100 fs is due to the developing bleach of the  $S_0$ – $S_n$

absorption, which contributes more at the high-energy side of the ESA band (Fig. 1b and 2). Whereas initially fast, the  $S_0$  hole broadens to  $\sim 2$  ps.

The hole dynamics can be quantitative characterized by analyzing the time-dependent GSB hole bandwidth (specifically, the half-width at half-maximum, hwhm).<sup>87,88</sup> Assuming that the hole replica is stationary, the hwhm evaluated at the short-wavelength side of the 990- and 1042-nm  $\Delta A$  features yields the time evolution of the ground-state hole. The bandwidth broadens with time for both Flav7 and Chrom7 from about 50 to 290  $\text{cm}^{-1}$ , which behavior can be described by a double exponential with time constants of  $\tau_1 = 230$  fs and  $\tau_2 = 1.0$  ps for Chrom7 and  $\tau_1 = 350$  fs and  $\tau_2 = 1.2$  ps for Flav7, Fig. 5. These time constants are also found in  $\Delta A$  kinetic traces within the  $S_0$ – $S_1$  absorption, Fig. 3 and Fig. S5–S8 (ESI<sup>†</sup>), but not outside this region, Fig. S7–S9 (ESI<sup>†</sup>). At wavelengths nearby the excitation wavelength (e.g., 980 nm, Chrom7, and 1060 nm, Flav7) these time constants describe the hole refilling (decay), whereas at those away (e.g., 840 nm, Chrom7, and 980 nm, Flav7) they describe the hole broadening (rise), Fig. 3. Within the outermost blue wing of the  $S_0$ – $S_1$  absorption spectrum, a faster initial hole dynamics is observed ( $-100$  and 0 fs  $\Delta A$  spectra, Fig. S10, ESI<sup>†</sup>), for which the fits yield a time constant of  $\tau_1 = 90 \pm 30$  fs for both Flav7 and Chrom7, Table S1 (ESI<sup>†</sup>). In an inhomogeneous ensemble, different members may have different lifetimes; probing across the blue wing interrogates the different, evidently steeper, portion of the  $S_0$  solute–solvent configurational potential, Fig. 5a. In the SE range, the double exponential decay is practically absent, e.g., at 1070 and 1120 nm for Chrom7 and 1140 and 1160 nm for Flav7 (Fig. 3), consistent with the notion that the hole replica is positioned at the minimum of the excited-state solute–solvent

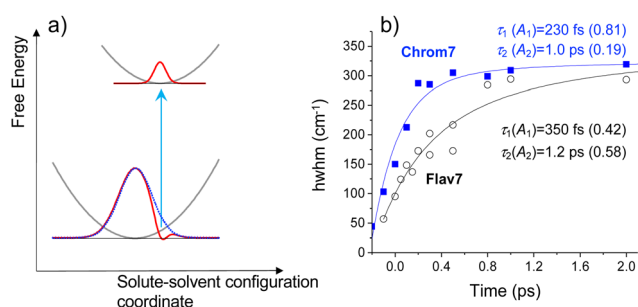


Fig. 5 (a) Schematic diagram for the hole relaxation when excitation is into the low-energy wing of the linear absorption spectrum and excites only a narrow range of resonant sites.<sup>84–86</sup> The distribution of excited-state population may only broaden without shift, but the ground-state population bleaches to fill the hole. In (b), for Chrom7 (excitation, 990 nm) and Flav7 (excitation, 1042 nm), the time evolution of the hwhm bandwidth evaluated at the short-wavelength side of the main negative  $\Delta A$  band is fitted to a two-exponential  $A_1 \exp(-t/\tau_1) + A_2 \exp(-t/\tau_2)$  function, with the fit curves and best-fit parameters shown.

configurational potential. The lack of red shift of the SE maximum is evidence that solvent stabilization of the excited  $S_1$ -solute is minor in these dyes.

Following 925-nm excitation, the high-energy-side ESA hwhm for Flav7 and Chrom7 evolves with  $\tau_1 \sim 120$  fs, which is the same as the  $90 \pm 30$  fs time constant within the accuracy, Table S1 (ESI<sup>†</sup>). This similarity may be explained by the fact that in cyanine dyes the  $S_0$  surfaces are typically much steeper than the  $S_1$  surfaces,<sup>38</sup> and therefore, although the  $S_1$  hole replica is not stationary following 0-1' excitation, the hwhm dynamics is predominantly determined by the gradient of the  $S_0$  solute-solvent configurational potential. The second component of the hole dynamics following 925-nm excitation remains about 1 ps for both dyes (Fig. S11–S16, ESI<sup>†</sup>).

Let us begin by interpreting  $\tau_2 = 1$  ps, which is independent of the dye nature and excitation wavelengths, and therefore, can be assigned to nonspecific solvent motion. This component matches the slow, 1.02 ps<sup>79</sup> time constant in the spectral response function for  $\text{CH}_2\text{Cl}_2$  obtained with a coumarin solute and assigned to diffusive solvation dynamics. Regarding  $\tau_1$ , there is no match of either 230 or 350 fs to the fast 144 fs<sup>79</sup> time constant due to inertial solvent dynamics in the same spectral response function. The 230 or 350 fs time constants are also significantly shorter than the average solvation time of  $\text{CH}_2\text{Cl}_2$ , 0.56 ps.<sup>79</sup> There is also no agreement with time constants of 0.57 and 2.21 ps due to solvent reorientation reported for neat  $\text{CH}_2\text{Cl}_2$  in ultrafast Raman-induced Kerr effect studies.<sup>89</sup> Therefore, the initial hole dynamics cannot be considered to be due to inertial solvation dynamics alone and also is not reducible to the rearrangement of the  $\text{CH}_2\text{Cl}_2$  molecules through their

rotational motion. Instead, one can propose the  $S_0$  site distribution with low-frequency ( $95\text{--}145\text{ cm}^{-1}$ ) skeletal deformations, such as torsional and bending vibrational modes known<sup>90</sup> to be optically active in polymethines. The 230- and 350-fs relaxation times are firmly within vibrational periods of these modes. An inhomogeneous ensemble in which different members exhibit a small, varying degree of deviation from the planarity has often been invoked to explain the absorption spectrum broadening in cyanine dyes.<sup>23,91,92</sup> Also, the link between torsional motion and hole burning dynamics was reported in barrierless excited-state relaxation of 1,1'-diethyl-2,2'-cyanine.<sup>69,93</sup> Skeletal deformations with somewhat higher vibrational frequencies of about  $350\text{ cm}^{-1}$  may be responsible for the 90-fs hole dynamics.

To determine vibrational relaxation rate constants for Chrom7 and Flav7 in the  $S_1$  state, the ESA  $\Delta A$  kinetic traces were fitted to a sum of multiexponential decay functions while including the known hole relaxation time constants. For 0-1' 925-nm excitation, this procedure yielded  $\sim 350$ -fs time constants for both dyes, Fig. S15 and S16 (ESI<sup>†</sup>). Spectral narrowing/broadening is a well-known indicator of vibrational energy flow,<sup>80–82</sup> and therefore, we also examined the time evolution of the ESA fwhm. For Flav7, a similar 323-fs time constant was found, Fig. S11 (ESI<sup>†</sup>). We note that vibrational relaxation manifests itself as the growth of the weaker peak relative to the major one in the ESA spectra (*cf.* the 300- and 500-fs  $\Delta A$  spectra, Fig. S17c and f, ESI<sup>†</sup>). A similar spectral change occurs during the fast hole dynamics, Fig. S10 (ESI<sup>†</sup>), which suggest that the involved low-frequency skeletal deformations also participate in the vibrational relaxation process. Vibrational relaxation was not observed after 990- and 1042-nm excitation.

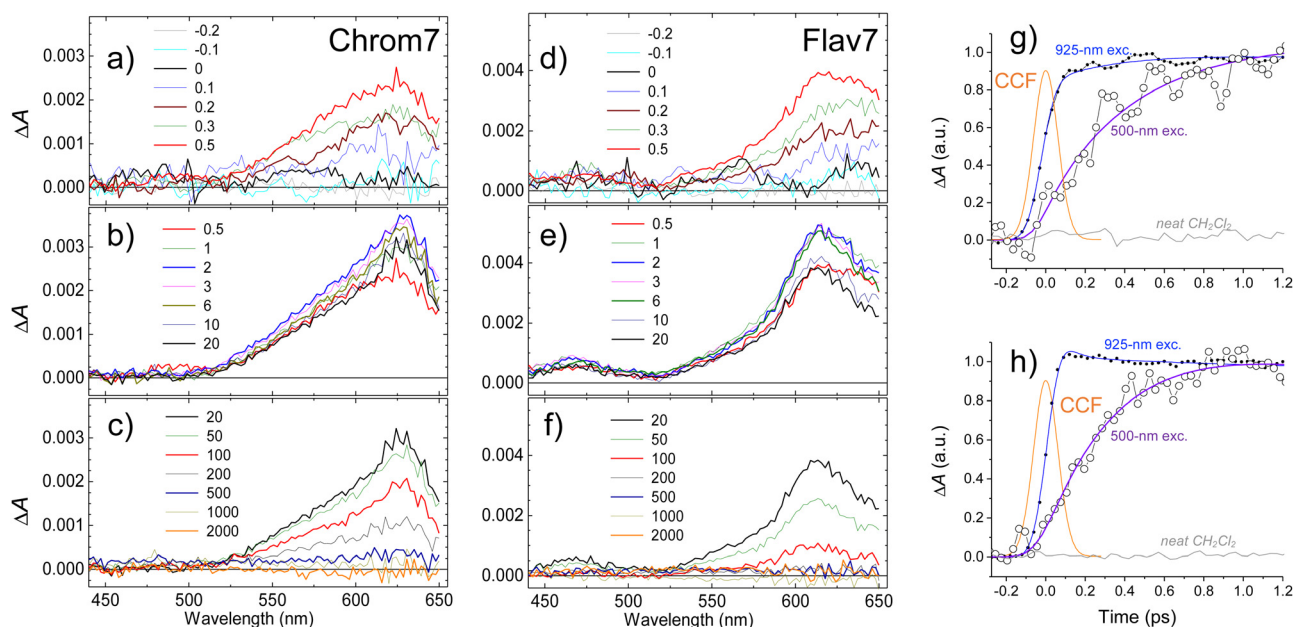


**Fig. 6** Transient absorption spectra of Chrom7 (a)–(c) and Flav7 (d)–(f) in  $\text{CH}_2\text{Cl}_2$  at short (a) and (d), intermediate (b) and (e), and long (c) and (f) times following 500-nm excitation. Delay times between the excitation and probe pulses are given in the legends. Representative  $\Delta A$  kinetics traces (symbols) at the probe wavelength of 575 nm for Chrom7 in (g) and 645 nm for Flav7 in (h) are compared with the data (symbols) measured following 925-nm excitation within the same ESA range: 553 nm in (g), and 659 nm in (h). The neat  $\text{CH}_2\text{Cl}_2$  yields a negligibly small  $\Delta A$  signal (as shown) under the same excitation conditions. The CCF between 500-nm excitation and probe pulses is Gaussian-shaped with a 145-fs fwhm, (g) and (h).

### Ultrafast transient absorption. 500-nm $S_n$ excitation

To provide an estimate for the lifetimes of highly-excited  $S_n$  electronic states, excitation of Chrom7 and Flav7 was carried out at 500 nm. The  $S_1$  ESA  $\Delta A$  signals rise with a significant delay within the first picosecond after excitation, Fig. 6 and Fig. S18, S19 (ESI<sup>†</sup>). The 300-fs  $\Delta A$  spectra are broadened, Fig. S20 (ESI<sup>†</sup>). The population in the  $S_1$  state becomes relaxed and thermalized at 6 ps because afterwards the  $\Delta A$  spectral shape remains unaltered with time and similar to that after  $S_1$  excitation. The amplitude of  $\Delta A$  signals decays to the noise level with the  $S_1$  lifetime, Table 1.

The entire  $\Delta A$  kinetic traces can be described by a triexponential decay model using deconvolution with the CCF. In addition to the  $S_1$  lifetime, two other time constants describe the initial  $\Delta A$  signal buildup and the spectral narrowing, Fig. S21 (ESI<sup>†</sup>). The buildup is interpreted as the  $S_1$  population rise following IC from the  $S_n$  state (time constant,  $0.40 \pm 0.05$  ps for Chrom7 and  $0.45 \pm 0.05$  ps for Flav7). Sub-picosecond  $S_n$  lifetimes were reported for other polymethines.<sup>94</sup> The narrowing (time constant,  $\sim 0.8$  ps, both dyes) is due vibrational relaxation in the  $S_1$  well bottom. Following  $S_n \rightarrow S_1$  IC,  $\sim 10\,000$   $\text{cm}^{-1}$  excess vibrational energy is deposited in the  $S_1$  state for Chrom7 and Flav7, which is  $\sim 10$  times more than produced by 925-nm excitation. Vibrational relaxation times are expected to be faster in higher vibrational states as reported for the indotricarbocyanine HITCI.<sup>95,96</sup> This expectation is transferrable provided that with an increase of vibrational energy the microscopic picture of energy transfer remains the same: *e.g.*, initially from solute's higher- to lower-frequency modes and then to solvent low-frequency modes, and other mechanisms, *e.g.*, from solute's high-frequency modes directly into high-frequency modes of the solvent, do not intervene.<sup>97</sup> The opposite trend in the vibrational relaxation times we observed (0.8 *vs.* 0.35 ps for 500- and 925-nm excitation, respectively) is because they characterize the arrival of hot population into the  $S_1$  well bottom and embody the transit times through all intermediate vibrational states involved.

### Vibrational coherences

Following  $S_0 \rightarrow S_1$  excitation of Chrom7 and Flav7, the oscillatory  $\Delta A$  signals occur predominantly in the  $S_1$  ESA region with the decoherence time constants of about 500 fs, Table S2 (ESI<sup>†</sup>). Following subtraction of exponential decays determined from the  $\Delta A$  fits, the oscillatory signals can be isolated and further analyzed by the fast-Fourier transform (FFT). The FFT analysis revealed several oscillation frequencies of 52, 139, and 278  $\text{cm}^{-1}$  for Chrom7 (excited at 990 nm) and 208 and 121  $\text{cm}^{-1}$  for Flav7 (excited at 1042 nm), Fig. S22a, b and S23a, b (ESI<sup>†</sup>). Upon 925-nm excitation of Chrom7, 104 and 208  $\text{cm}^{-1}$  FFT bands, in addition to the one at 52  $\text{cm}^{-1}$ , were detected (Fig. S23g and h, ESI<sup>†</sup>). For Flav7, a 225  $\text{cm}^{-1}$  FFT band (Fig. S22g and h, 925-nm excitation, ESI<sup>†</sup>) is thought to be the same as the 208  $\text{cm}^{-1}$  band observed following 1042-nm excitation based on the accuracy of data analysis.

The coherent motion observed most likely takes place in the  $S_1$  and not  $S_0$  state because the absorption from  $S_1$

predominates throughout the ESA probing region. Ultrafast pulse excitation prepares the molecule in the FC electronic state in a superposition of optically active vibrational levels called a wavepacket. The vibrational wavepacket oscillates between the inner and outer turning points of the excited-state potential. As a result, the oscillations occur with a  $\pi$ -shift in the red and blue wings of the  $S_1$  ESA band, as observed, Fig. S24 (ESI<sup>†</sup>). Excitation at the low-energy side of the absorption spectrum is known to suppress vibrational coherence in the  $S_1$  state,<sup>98,99</sup> which agrees with the oscillations for Chrom7 and Flav7 in this case being less pronounced than for 0-1' 925-nm excitation. Upon 500-nm  $S_n$  excitation of Chrom7, the sub-1 ps  $\Delta A$  signal rise is superimposed with 139- $\text{cm}^{-1}$  modulations, Fig. S25 (ESI<sup>†</sup>). Product vibrational coherence may result from crossing of PESs itself<sup>100</sup> or be transferred from the initial state following its preparation by a short excitation pulse. In polymethine dyes, vibrational coherence in  $S_1$  following IC from  $S_n$  was observed for the first-time, to our knowledge, in indolenine HDITC following the deposition into  $S_1$  chemically significant  $\sim 1.5$  eV of energy,<sup>101</sup> similar to the amount for Chrom7. No coherence was observed after 500-nm excitation of Flav7.

Vibrational wavepackets were ubiquitously observed in polymethine dyes following ultrafast pulse excitation.<sup>93,98,99,101-109</sup> Whereas in many instances the coherence observed was merely due to 'spectator' optically-active vibrational levels, for Cy5 the 273  $\text{cm}^{-1}$  vibrational mode connecting the planar FC and photoisomerization transition state structures was claimed to be involved.<sup>105</sup> Several studies demonstrated that vibrational coherence can control the photoisomerization quantum yield,<sup>110-112</sup> which was interpreted as altering the excited-state relaxation path towards the CI seam separating the parent and the photoisomer forms.<sup>90</sup> In 1,1'-diethyl-2,2'-cyanine, vibrational coherences in Raman-active 200  $\text{cm}^{-1}$  butterfly-like symmetric stretching as well as 130 and 300  $\text{cm}^{-1}$  bending modes play a role.<sup>111,112</sup> The prominent 52, 139, 104, 208, and 278  $\text{cm}^{-1}$  vibrational modes observed in our work are in the same frequency range as the modes previously proposed to be involved in the photoisomerization pathway.

### Lowest-energy triplet states

We performed phosphorescence measurements of Chrom7 and Flav7 in a frozen solvent matrix at 77 K following 532-nm 7-ns pulsed excitation to locate the energy position of lowest-energy triplet  $T_1$  states. No phosphorescence was observed in ethanol glass. A heavy-atom containing matrix ( $\text{CD}_3\text{I}$ ) was then used to increase the ISC and radiative phosphorescence rates. Also, deuterated solvents may reduce possible non-radiative deactivation of low-energy excited states *via* coupling to C-H vibrational modes of the surrounding medium and are often preferred for near-IR luminescence measurements. The excitation of Chrom7 in a  $\text{CD}_3\text{I}$  matrix at 77 K resulted in weak phosphorescence with a maximum at 1305 nm, Fig. 7a. The  $\sim 1260$ -nm shoulder is assigned to  $^1\text{O}_2$  emission,<sup>72</sup> whereas the feature at 1110 nm is due to contributions from scattered fundamental (1064 nm) laser light and  $\text{CD}_3\text{I}$  matrix emission,

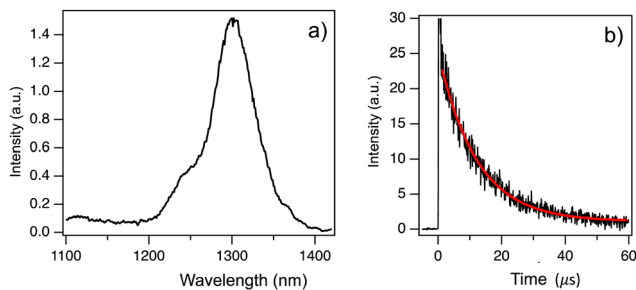


Fig. 7 Phosphorescence spectrum for Chrom7 in a CD<sub>3</sub>I matrix at 77 K, (a) The phosphorescence was recorded in the 4–19 μs time interval after pulsed laser excitation (532 nm, 7-ns pulse width). The phosphorescence decay (black) was measured at a 1300-nm wavelength and can be fitted to a single exponential decay (red) with a 12 μs lifetime, (b).

Fig. S26 (ESI<sup>†</sup>). The phosphorescence intensity decayed mono-exponentially with a lifetime of 12 μs, Fig. 7b. Nanosecond pulsed excitation of Flav7 in a CD<sub>3</sub>I matrix (77 K) either at 532 nm or 1064 nm did not result in any detectable phosphorescence in the 1000–1400 nm range. A possible reason is that Flav7 phosphorescence occurs at wavelengths longer than the 1400 nm PMT detection limit. This implies a lower T<sub>1</sub> state in Flav7 than in Chrom7, which is consistent with the lower S<sub>1</sub> state in Flav7 than in Chrom7. The absence of phosphorescence from Flav7 might also have been caused by poor triplet state population and/or a very low phosphorescence radiative rate constant. The first cause is unlikely; provided that about a factor of 2.5 difference in the S<sub>1</sub> lifetimes between Chrom7 and Flav7 transfers into the S<sub>1</sub> → T<sub>1</sub> ISC quantum yields, the T<sub>1</sub> population in Flav7 would still be measurable. The second explanation is also unlikely because of the similar radiative rate constants in these two dyes (Table 1), which implies a similar electronic nature of the low-energy excited states.

The energy of the T<sub>1</sub> state may in principle be determined from the position of the highest-energy phosphorescence vibronic band.<sup>56</sup> If, however, the phosphorescence spectrum does not show sufficiently resolved vibronic structure, the ‘onset’ of the short-wavelength portion of the phosphorescence spectrum

may be used to estimate the upper limit of the T<sub>1</sub> state energy.<sup>56</sup> Neither of these two approaches work for Chrom7 because of the lack of vibronic structure and the presence of O<sub>2</sub> emission. Instead, a 0.9 level at which the 0–0' vibronic bands of absorption and fluorescence spectra cross (S<sub>0</sub>–S<sub>1</sub> energy gap), Fig. 1, was adopted for the 1305-nm phosphorescence band, which yields the intersection at 1290 nm and thus the T<sub>1</sub> energy at 7750 cm<sup>-1</sup> above S<sub>0</sub>. Based on the 1400-nm detection limit, the Flav7 T<sub>1</sub> state is placed at 7140 cm<sup>-1</sup> or lower.

### Temperature dependence of the S<sub>1</sub> state lifetime

The fluorescence quantum yields, Φ<sub>f</sub>, and the S<sub>1</sub>-state lifetime, τ<sub>f</sub> for Chrom7 and Flav7 rise upon lowering the temperature before reaching a plateau, Fig. S27–S29 (ESI<sup>†</sup>), and Fig. 8. The total non-radiative rate constant in the S<sub>1</sub> state, k<sub>nr</sub>, is given by:<sup>27,33,46</sup>  $k_{nr} = k_{ic} + k_{ph} = (1/\Phi_f - 1) \cdot k_{rad} = 1/\tau_f - k_{rad}$ . Here, k<sub>rad</sub> and k<sub>ic</sub> are the practically temperature independent radiative and direct IC rate constants, and k<sub>ph</sub> is the rate constant for photoisomerization barrier crossing, which is temperature and solvent viscosity dependent according to the following equation:  $k_{ph} = D\zeta^{-a} \exp(-E_0/RT)$ . Here, R is the universal gas constant, T is the absolute temperature, E<sub>0</sub> is the intrinsic barrier height, ζ is the solvent viscosity, and D and a are the parameters, where a (0 ≤ a ≤ 1) depends on the size and shape of the intrinsic barrier,<sup>113–115</sup> reaching the low limit for larger barriers.<sup>116,117</sup> The approximation used in many studies<sup>48,116–121</sup> is that in a narrow temperature range,  $\zeta = \zeta_0 \exp(E_\zeta/RT)$ ,<sup>122</sup> where ζ<sub>0</sub> is the constant, and E<sub>ζ</sub> is the solvent viscosity activation energy. As a result, k<sub>ph</sub> obeys the Arrhenius equation,  $k_{ph} = A \exp(-E_a/RT)$ , with the preexponential factor A and the activation energy E<sub>a</sub> given by  $E_a = E_0 + aE_\zeta$ . When plotted against T<sup>-1</sup>, k<sub>nr</sub> should exhibit the slope defined by E<sub>a</sub> before reaching a plateau defined by k<sub>ic</sub> at low T. The k<sub>nr</sub> values determined from the measured Φ<sub>f</sub> and τ<sub>f</sub> are fitted to a sum of k<sub>ph</sub> and k<sub>ic</sub>, Fig. 8. At 22 °C, the fits for Chrom7 yield k<sub>ic</sub> = 4.03 × 10<sup>9</sup> s<sup>-1</sup>, which is larger than k<sub>ph</sub> = 5.72 × 10<sup>8</sup> s<sup>-1</sup> by a factor of 7, but for Flav7 the difference is not dramatic as k<sub>ic</sub> = 8.89 × 10<sup>9</sup> s<sup>-1</sup> is larger than k<sub>ph</sub> = 3.88 × 10<sup>9</sup> s<sup>-1</sup> only by a factor of 2.3. The fits yield reasonable A = 6.97 × 10<sup>12</sup>



Fig. 8 Chrom7, (a) and Flav7, (b) in CHCl<sub>3</sub>: influence of temperature on the inverse S<sub>1</sub>-state lifetime, where τ<sub>f</sub> values were measured by femtosecond transient absorption (open circles) and calculated from the fluorescence quantum yields (solid circles) assuming that k<sub>rad</sub> is the same as in CH<sub>2</sub>Cl<sub>2</sub>, Table 1, and the best fits of the 1/τ<sub>f</sub> data using the Arrhenius k<sub>ph</sub> and temperature independent k<sub>ic</sub> and k<sub>rad</sub> rate constants. The insets show the rate constants and CHCl<sub>3</sub> viscosity, labelled E<sub>ζ</sub> (for comparison, the ζ values were scaled by a constant factor), plotted on a natural logarithmic scale vs. 10<sup>3</sup> T<sup>-1</sup>.

and  $5.29 \times 10^{12} \text{ s}^{-1}$  for Chrom7 and Flav7, respectively, as well as  $E_a = 5.20 \pm 0.75$  and  $4.26 \pm 0.74 \text{ kcal mol}^{-1}$ , which are much larger than  $E_c$  of  $\text{CHCl}_3$ . The latter is estimated to be  $1.78 \text{ kcal mol}^{-1}$  based on viscosities<sup>123</sup> reported between  $-25$  and  $50 \text{ }^\circ\text{C}$ , which is about the temperature range investigated in this work.

Fig. 9 summarizes the  $S_1$  radiationless relaxation mechanism we propose for the SWIR polymethine dyes studied in this work, which involves competing energy gap and isomerization decay pathways. Several conclusions can be made. First, the application of energy gap theories for unconstrained SWIR polymethine dyes, which does not account for  $k_{\text{ph}}$  while silently assuming that the nonradiative decay is entirely due to direct IC,<sup>20,124</sup> may be in error. Compared to the fit<sup>124</sup> of  $k_{\text{nr}}$  alone to the energy gap model, plotting  $k_{\text{nr}} - k_{\text{ph}}$  produces a better fit. Second, the difference in room-temperature lifetimes for Chrom7 and Flav7 upon going from  $\text{CH}_2\text{Cl}_2$  to  $\text{CHCl}_3$  (Table 1) cannot be attributed to the gap law alone because the solvatochromic shifts involved are small ( $\sim 3 \text{ nm}$ ). Shorter  $S_1$  lifetimes in  $\text{CH}_2\text{Cl}_2$  are consistent with the presence of the photoisomerization pathway less hindered by a less viscous solvent ( $0.42$  and  $0.56 \text{ cP}$  for  $\text{CH}_2\text{Cl}_2$  and  $\text{CHCl}_3$ , respectively,  $20 \text{ }^\circ\text{C}$ ). Third, it is reasonable to assume that the solvent contribution to  $E_a$  is similar for Flav7 and Chrom7 because the measured activation energies are not much different.<sup>114–117</sup> This suggests that the intrinsic photoisomerization barrier is somewhat larger in Chrom7 than Flav7. This is consistent with Chrom7 having a bulkier 2-alkyl group as compared to a phenyl group in Flav7. A slowing down of the  $S_1$  photoisomerization with increasing bulkiness of the twisting fragment was previously observed.<sup>125,126</sup>

Finally, one can compare  $k_{\text{ph}}$ ,  $k_{\text{ic}}$ , and  $E_a$  values found in this work with those reported in the  $S_1$  state for heptamethine cyanine dyes. For HITCI (in DMSO unless indicated otherwise), direct IC is slow,  $k_{\text{ic}} = 2.8 \times 10^8 \text{ s}^{-1}$ ,<sup>33</sup> as expected because its

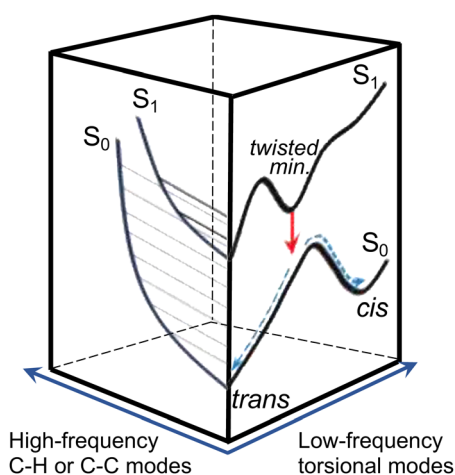


Fig. 9 The radiationless relaxation mechanism of the SWIR polymethine dyes studied in this work with the competing pathways of direct IC, which takes place within the planar  $S_1$  *trans*-form and obeys the energy gap law, and photoisomerization, which is thermally activated. The photoisomerization motion predominantly samples the *trans*-side of the twisted  $S_1$  minimum and is essentially nonreactive.

absorption maximum is blue shifted by  $\sim 260 \text{ nm}$  compared to Flav7 and Chrom7. The photoisomerization activation energies,  $5.3$  (HITCI<sup>33</sup>),  $5.0$  (DTTCI<sup>34</sup>), and  $6.0$  (IR-140<sup>34</sup>)  $\text{kcal mol}^{-1}$  as well as  $3.5$  (DTTCI<sup>34</sup>),  $4.5$  (IR-140<sup>34</sup>), and  $5.74$  (DOTCI<sup>48</sup>)  $\text{kcal mol}^{-1}$  in  $\text{C}_2\text{H}_5\text{OH}$  are comparable with the  $E_a$  values in Flav7 and Chrom7. Similar activation energies were measured for photoisomerization of dicarbocyanine dyes.<sup>48,76</sup> Photoisomerization is the major  $S_1$  relaxation pathway in heptamethine cyanine dyes, e.g., the  $k_{\text{ph}}\tau_f$  quantum yield is  $\sim 0.7$  in HITCI ( $k_{\text{ph}} = 3.3 \times 10^8 \text{ s}^{-1}$ <sup>33</sup>). Photoisomer quantum yields are about  $0.08$  in penta- and heptamethine cyanines,<sup>30–32,40</sup> which based on  $k_{\text{ph}}\tau_f$  in these dyes yields a branching ratio  $\phi$  of  $\sim 0.1$ , Fig. 1a. The values of  $k_{\text{ph}}$  in Chrom7 and Flav7 are significant ( $5.72 \times 10^8 \text{ s}^{-1}$  and  $3.88 \times 10^9 \text{ s}^{-1}$ ), so that  $k_{\text{ph}}\tau_f$  becomes  $0.12$  and  $0.3$ , that is still significant, and which for the photoisomer quantum yields estimated,  $1.8 \times 10^{-3}$  and  $6.4 \times 10^{-3}$ , suggests the branching ratio of  $0.014$  and  $0.02$  in Chrom7 and Flav7, respectively, Table S3 (ESI<sup>†</sup>). This is 10 times smaller compared with penta- and heptamethine dyes. Quantum chemical computations of polymethine dyes suggest the presence of the  $S_1/S_0$  CI seam on the *trans*-side in the vicinity of the  $S_1$ -state twisted minimum.<sup>38,39</sup> One then can propose that Chrom7 and Flav7, after overcoming the photoisomerization barrier, reach the seam region where local topology even more strongly favors the  $S_0$ -*trans* nonreactive channel over  $S_0$ -*cis* product formation.

### Highly excited states and implications for bioimaging

After SE becomes spectrally separated from the absorption and unaffected over time in the femto-to-picosecond range, the  $\sigma_{\text{SE}}(\lambda)$  spectrum can be constructed from the steady-state fluorescence spectrum,<sup>127,128</sup> Fig. 1. When vibrational relaxation in  $S_0$  is faster compared with the  $S_1$  lifetime and in the absence of an appreciable photochemical change, which are valid assumptions based on the data, the  $\Delta A(\lambda, t)$  spectrum is:  $\Delta A(\lambda, t) = \text{constant} \cdot n_{S_1}(t) \cdot (-\sigma_A(\lambda) - \sigma_{\text{SE}}(\lambda) + \sigma_{\text{ESA}}(\lambda))$ , where  $n_{S_1}(t)$  is the  $S_1$  population at a delay time  $t$ . The measured  $\Delta A(\lambda, t)$  spectrum can be scaled to a sum of  $\sigma_A(\lambda)$  and  $\sigma_{\text{SE}}(\lambda)$  with the minimal uncertainty using the wavelength range where the spectrum and the sum closely match each other (implying that  $\sigma_{\text{ESA}}(\lambda) \sim 0$  in this range) and change rapidly; the excess of the scaled  $\Delta A(\lambda, t)$  over  $\sigma_A(\lambda) + \sigma_{\text{SE}}(\lambda)$  outside the matching range yields the unknown  $\sigma_{\text{ESA}}(\lambda)$  spectrum. The said wavelength range is present between  $875$ – $970 \text{ nm}$  for Chrom7 and  $960$ – $1020 \text{ nm}$  for Flav7. Consequently, the  $\sigma_{\text{ESA}}(\lambda)$  spectra were determined, Fig. 10, with the accuracy of the  $\sigma_{\text{ESA}}(\lambda)$  values estimated to be better than  $50\%$ .

Both Chrom7 and Flav7 exhibit an intense ESA band in the SWIR range ( $1000$  and  $1050 \text{ nm}$ , respectively), which is somewhat red-shifted with respect to the  $S_0$ - $S_1$  absorption maximum, as well as weak ESA in the near-IR region, Fig. 10. We attribute these two ESA features to the terminal  $S_2$  and  $S_3$  states, although we cannot exclude the possibility of singlet excited states lying even lower. Blue-shifted, intense ESA (Fig. 10) resembles that in other symmetric long-chain cyanines<sup>129</sup> and assigned to the terminal  $S_{4,5}$  states (dual peaks at  $683$  and

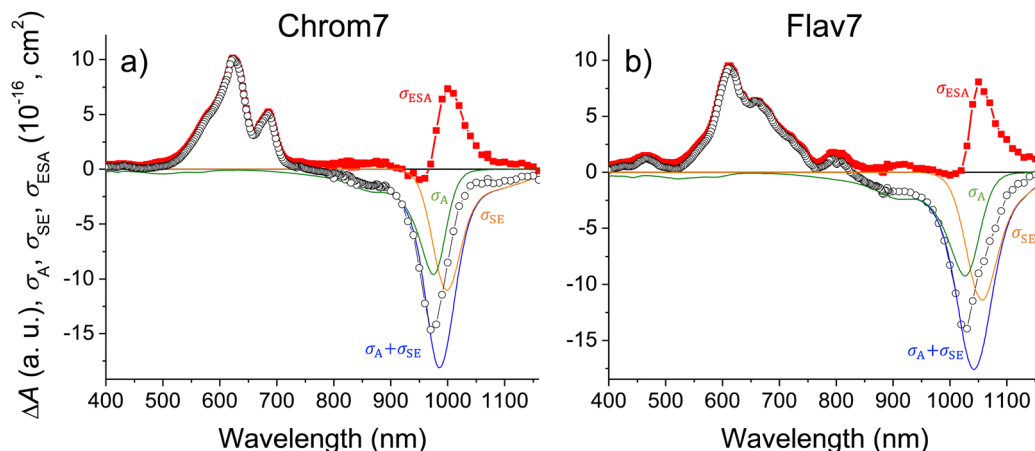


Fig. 10 Chrom7 excited at 990 nm, (a) and Flav7 excited at 1042 nm, (b) for which the 50-ps  $\Delta A$  spectrum from Fig. 2 is scaled (open symbols) to the  $\sigma_A(\lambda) + \sigma_{SE}(\lambda)$  sum (with the individual  $\sigma_A(\lambda)$  and  $\sigma_{SE}(\lambda)$  contributions shown); their difference (solid symbols) is equal to the  $\sigma_{ESA}(\lambda)$  spectrum of ESA from  $S_1$ . The  $\sigma_{ESA}(\lambda)$  spectral shape is found to be constant from  $\sim 100$  ps to delay times as short as 500 fs, Fig. S30 (ESI $\dagger$ ).

622 nm for Chrom7, and 657 and 612 nm for Flav7). Incidentally, the peak separation gap of 1435 and 1120  $\text{cm}^{-1}$  is not overwhelmingly larger than the  $\sim 1230$   $\text{cm}^{-1}$  frequency of the optically active vibrational mode of the  $S_0$ - $S_1$  transition, Fig. 1. The transition energies of ESA from the equilibrated  $S_1$  state, when they are adjusted for the  $S_0$ - $S_1$  energy gap (10 140 and 9700  $\text{cm}^{-1}$  for Chrom7 and Flav7) are expected to match the  $S_0$ - $S_n$  band positions. We found the terminal  $S_2$  and  $S_{4,5}$  states to be close (within 120–240  $\text{cm}^{-1}$  for  $S_2$  and 300–800  $\text{cm}^{-1}$  for  $S_{4,5}$ ) to the visible band maxima in the linear absorption spectrum, Fig. S31 (ESI $\dagger$ ). We note that the ESA bands are much narrower than the diffuse  $S_0$ - $S_n$  absorption bands. Similar effects were

observed for ESA of coumarin C153<sup>130</sup> and HITCI,<sup>131</sup> and may be attributed to either fewer vibrational modes being optically active in  $S_1$  compared to  $S_0$ <sup>130</sup> and/or the presence of several closely-lying excited states where intense absorption from  $S_1$  is only allowed to occur into one of them.<sup>132</sup> The energy diagrams for Chrom7 and Flav7 are summarized in Fig. 11.

The  $\sigma_{ESA}(\lambda)$  values in two major bands are  $8.1 \times 10^{-16}$   $\text{cm}^2$  at 1050 nm and  $9.2 \times 10^{-16}$   $\text{cm}^2$  at 612 nm for Flav7 and  $7.3 \times 10^{-16}$   $\text{cm}^2$  at 1000 nm and  $\sigma_{ESA} = 9.8 \times 10^{-16}$   $\text{cm}^2$  at 622 nm for Chrom7. Consideration of the ESA spectrum is important for Flav7 and Chrom7, as well as generally for molecular probes in high-intensity photonic applications and measurements, e.g., fluorescence correlation spectroscopy<sup>18,133,134</sup> where the fluorophore  $S_0 \rightarrow S_1$  excitation rate constant (intensity times cross-section) may become comparable with the inverse  $S_1$  lifetime. The  $S_1$  population may then be promoted by secondary excitation into one of the higher electronically excited states, which usually is much more prone to molecular decomposition compared to  $S_1$ . Also,  $S_n$  may exhibit a very different photo-reactivity. Facile photoisomerization<sup>135,136</sup> and ISC<sup>137</sup> in  $S_n$  states of polymethine dyes were reported. High-intensity irradiation, such as 25 kW peak power focused into a micrometer spot typical for two-photon microscopy,<sup>138</sup> of Flav7 and Chrom7 in the 1050- and 1000-nm region should cause, at least, the  $S_0 \rightarrow S_1 \rightarrow S_2$  excitation based on comparable intensity times cross-section products of the  $S_0 \rightarrow S_1$  and  $S_1 \rightarrow S_2$  steps. In the case of pulsed visible irradiation utilized in confocal microscopy, biphotonic excitation may also be expected if the used irradiation wavelength overlaps the visible ESA. On the other hand, irradiation of Flav7 between 820 and 1020 nm and Chrom7 between 730 and 910 nm limits the population promotion further than the  $S_1$  state because ESA in these regions is weak.

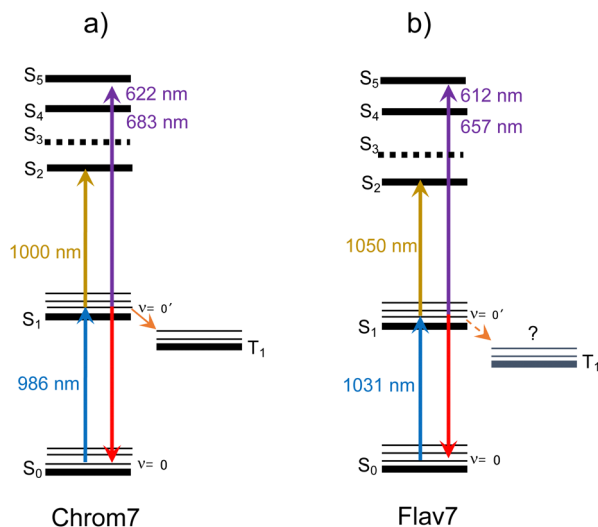


Fig. 11 Energy diagram for Chrom7, (a) and Flav7, (b) based on this work. The  $S_0$ - $S_1$  energy gap is 10 140 and 9700  $\text{cm}^{-1}$  based on the overlap of the  $0-0'$  absorption and fluorescence bands at 986 and 1031 nm. The  $S_1 \rightarrow S_2$  and  $S_0 \rightarrow S_1$  transitions occur at nearly the same energy, and the  $S_5$  states are found to be within 100  $\text{cm}^{-1}$  of each other at  $\sim 26150$   $\text{cm}^{-1}$ . The  $S_3$  position is only tentatively shown because near-IR ESA attributed to the  $S_1 \rightarrow S_3$  transition is weak and diffuse. The  $T_1$  state is at 7750  $\text{cm}^{-1}$  above  $S_0$  for Chrom7 and is assumed, see the text, at 7140  $\text{cm}^{-1}$  or lower for Flav7.

## Conclusions

We have characterized the ultrafast dynamics as well as photo-physical and photochemical properties of a chromenylium and

a flavylum polymethine dye the latter of which is one of the brightest organic SWIR emitters reported to date. By using different excitation wavelengths, the separation of dynamic inhomogeneous broadening of vibronic spectra and intramolecular vibrational relaxation was made possible, as well as the characterization of ultrafast deactivation of highly excited electronic states. The complexity of deactivation of the first excited singlet state ( $S_1$ ) is revealed by excited-state lifetime and time-resolved phosphorescence measurements at different temperatures. Intersystem crossing is found not to impact room-temperature excited-state relaxation. The results highlight the presence of two competing radiationless relaxation mechanisms in  $S_1$ . One with the minimal temperature sensitivity is internal conversion *via* energy gap law. Another is twisting about one of the carbon-carbon conjugated bonds, which has an excited-state Arrhenius activation energy comparable to that of photoisomerization in symmetric penta- and heptamethine cyanines and permits traces of isomer products. Direct internal conversion predominates thermally-activated twisting in the studied SWIR dyes at room temperature, but the latter pathway is substantial, constituting  $\sim 15$ – $40\%$  of the total relaxation rate constant, suggesting that the SWIR fluorophore brightness can be further improved by conformational constraints. The knowledge of excited-state absorption is important in the design of fluorophores for biological and medical applications because it may reduce their brightness thereby limiting their potential in imaging application. The understanding of photoproperties is overall crucial in the design of organic fluorophores.

## Experimental

### Materials

Anhydrous dichloromethane (EMD Millipore, ACS grade) was used as a solvent, and in a few cases, chloroform was used. Chrom7 and Flav7 were synthesized by and received from Dr E. Sletten (UCLA).<sup>24,25</sup> UV-vis absorption spectra of the solutions were measured using a Varian Cary 50 Bio spectrophotometer.

### Photoluminescence experiments

Temperature dependent fluorescence spectra following 900-nm irradiation were recorded on a FLS1000 spectrometer (Edinburgh Analytical Instruments) in conjunction with a H10330B-45 near-IR sensitive PMT (Hamamatsu). The sample solutions in  $1 \times 1 \text{ cm}^2$  quartz cells were deoxygenated before measurements.  $\text{CHCl}_3$  (Acros, spectroscopic grade) was used as a solvent instead of  $\text{CH}_2\text{Cl}_2$  because of a higher boiling point of the former. In conjunction with these experiments, steady-state absorption spectra were recorded on an Agilent 8453 spectrometer equipped with a Peltier temperature-controlled sample holder (PTP-1, PerkinElmer) in 1-cm pathlength quartz cells.

Phosphorescence measurements were performed on a modified Fluorolog-3 spectrometer (HORIBA Jobin Yvon) in conjunction with a near-IR sensitive photomultiplier (H10330A-45, Hamamatsu). A Spectra-Physics GCR-150-30

Nd:YAG laser (532 nm, 7-ns pulse width or 1064 nm, 10-ns pulse width) was used for excitation ( $< 2 \text{ mJ pulse}^{-1}$ ). For recording time-resolved phosphorescence spectra, the signal from the near-IR sensitive PMT was time gated using a SR250 Boxcar Integrator (Stanford Research Systems) and digitized in the Fluorolog-3 SPECTRACQ unit through a DM303M Voltage Input Module (HORIBA Jobin Yvon). Phosphorescence decay was measured with the near-IR sensitive PMT and stored using a digital oscilloscope (TDS 360, Tektronics). The sample solutions were placed in 4-mm (outer diameter) quartz tubes, deoxygenated by purging with  $\text{N}_2$  gas and frozen in an optically-transparent quartz liquid  $\text{N}_2$  Dewar (77 K) located inside the sample chamber of the spectrometer.

### Nanosecond transient absorption

The previously described set-up<sup>139</sup> used 532-nm 7-ns excitation pulses produced by the GCR-150-30 Nd:YAG laser and an Xe-arc lamp as a probing source. Solutions of Chrom7 were prepared in  $1 \times 1 \text{ cm}^2$  quartz cells at concentrations such that the absorbance was  $\sim 0.3$  at the excitation wavelength.

### Ultrafast transient absorption

The details of the set-up and experimental procedures can be found in ESI,† section. Briefly, the set-up used<sup>140,141</sup> is based on a regeneratively amplified Ti:sapphire laser system producing a 1 kHz train of 90 fs (fwhm) pulses with 0.9 mJ of energy centered at 800 nm. The 50% portion of the amplified output is sent to an optical parametric amplifier (OPA) to produce 1042-, 990-, and 925-nm and 500-nm pulses used for sample excitation. The remaining half was used either to produce a broadband white-light continuum (wlc) probe light in the 340–935 nm range or to pump another OPA to generate a single-wavelength probe light tunable from 800 to 1160 nm. The polarization plane of the excitation light was set to the magic angle ( $54.7^\circ$ ) with respect to that of the probe light to eliminate rotational reorientation effects from transient absorption signals. The probe and excitation beams overlapped at a  $6^\circ$  angle at the sample position, being 60 and 200  $\mu\text{m}$  in diameter. The excitation energy was attenuated to around 45–60 nJ  $\text{pulse}^{-1}$  to ensure that single-photon excitation is responsible for the measured  $\Delta A$  data, Fig. S32 (ESI†). The experiments were performed at  $22^\circ \text{C}$  unless stated otherwise and utilized a 2-mm pathlength rotating cell. The absorption spectra of Flav7 and Chrom7 samples obeyed the Lambert-Beer law and showed no change after laser experiments. The  $\Delta A$  data were corrected for group-velocity dispersion in the wlc probe light with a 20-fs accuracy using electronic instantaneous response of the  $\text{CH}_2\text{Cl}_2$  solvent<sup>142,143</sup> present within the initial  $\sim 170$  fs after excitation, Fig. S33a–c (ESI†). The CCF between the excitation pulse and spectral components of the wlc pulse (Gaussian-shaped with fwhm of 125 fs for 990- and 1042-nm excitation, and 145 fs for 925-nm excitation) was determined using the same solvent response as described in the literature.<sup>142</sup> The CCF between 500-nm and wlc probe pulses (Gaussian, 145-fs fwhm, Fig. S33d, ESI†) was determined using the solvent anti-Stokes  $\Delta A$  signal at 433 nm at time zero<sup>144</sup> due

to the Raman-active C–H stretching mode of CH<sub>2</sub>Cl<sub>2</sub> (3045 cm<sup>-1</sup><sup>45</sup>). When probing in the near-IR using the OPA, the time zero and CCF (fwhm, 155 fs) were determined *via* sum-frequency mixing of the excitation and probe light in a 0.1-mm thick, type-I BBO crystal, Fig. S34 (ESI†). The representative  $\Delta A$  kinetic traces were fitted with CCF deconvolution to a sum of up to six exponential decay functions,  $\Delta A = \sum_{i=6} A_i(\lambda)e^{-\frac{t}{\tau_i}}$ , where  $A_i(\lambda)$  is the amplitude and  $\tau_i$  is the time constant of the  $i$ th component. From multiexponential fits with CCF deconvolution the time resolution of the experiments reported herein is 40 fs. FFT analysis was performed on the residuals of multiexponential fits.

The same set-up with wlc probing was used for low-temperature S<sub>1</sub>-state lifetime measurements. Excitation was at 1042 nm (Flav7) and 990 nm (Chrom7). CHCl<sub>3</sub> was used as a solvent (ACS-grade anhydrous, Fischer Scientific). The samples were kept in a 1 × 1 × 4 cm<sup>3</sup> quartz cell immersed into a Dewar condenser filled with acetone cooled by liquid N<sub>2</sub>, where the temperature was monitored with a thermocouple.

## Author contributions

L. M. Obloy: femtosecond pump–probe experiments, data analysis, and manuscript writing; S. Jockusch: temperature-dependent absorption and emission experiments and data analysis; A. N. Tarnovsky: work proposal and organization, femtosecond pump–probe experiments, data analysis, and manuscript writing. All the authors participated in the discussions and contributed writing and preparation of the manuscript.

## Conflicts of interest

There are no conflicts to declare.

## Acknowledgements

In memory of T. K. Razumova (1932–2023), whose work advanced the understanding of photoprocesses in polymethine dyes and who was the graduate advisor of ANT. The authors acknowledge Emily D. Cosco and Ellen M. Sletten for providing Flav7 and Chrom7 and critical reading of the manuscript. The authors are also thankful to George T. Lawton for his help with the 925-nm transient absorption experiments. This work is supported by the National Science Foundation (CHE-2102619, CHE-0923360, and CHE-1626420).

## Notes and references

- 1 E. Thimsen, B. Sadtler and M. Y. Berezin, Shortwave-infrared (SWIR) Emitters for Biological Imaging: a Review of Challenges and Opportunities, *Nanophotonics*, 2017, **6**, 1043–1054.
- 2 S. M. Usama and K. Burgess, Hows and Whys of Tumor-Seeking Dyes, *Acc. Chem. Res.*, 2021, **54**, 2121–2131.

- 3 V. G. Bandi, M. P. Luciano, M. Saccomano, N. L. Patel, T. S. Bischof, J. G. P. Lingg, P. T. Tsrunchev, M. N. Nix, B. Ruehle, C. Sanders, L. Riffle, C. M. Robinson, S. Difilippantonio, J. D. Kalen, U. Resch-Genger, J. Ivanic, O. T. Bruns and M. J. Schnermann, Targeted Multicolor In Vivo Imaging over 1000 nm Enabled by Nonamethine Cyanines, *Nat. Methods*, 2022, **19**, 353–358.
- 4 M. P. Coogan and V. Fernandes-Moreira, Progress with, and Prospects for, Metal Complexes in Cell Imaging, *Chem. Commun.*, 2014, **50**, 384–399.
- 5 S. Li, J. Wei, Q. Yao, X. Song, J. Xie and H. Yang, Emerging Ultrasmall Luminescent Nanoprobes for In Vivo Bioimaging, *Chem. Soc. Rev.*, 2023, **52**, 1672–1696.
- 6 M. J. Schnermann, Organic Dyes for Deep Bioimaging, *Nature*, 2017, **551**, 176–177.
- 7 A. Waggoner, Fluorescent labels for proteomics and genomics, *Curr. Opin. Chem. Biol.*, 2006, **10**, 62–66.
- 8 B. A. Armitage, Cyanine Dye-DNA Interactions: Intercalation, Groove Binding, and Aggregation, *Top. Curr. Chem.*, 2005, **253**, 55–76.
- 9 M. Levitus and S. Ranjit, Cyanine Dyes in Biophysical Research: The Photophysics of Polymethine Fluorescent Dyes in Biomolecular Environments, *Q. Rev. Biophys.*, 2011, **44**, 123–151.
- 10 A. P. Gorka, R. R. Nani and M. J. Schnermann, Cyanine Polyene Reactivity: Scope and Biomedical Applications, *Org. Biomol. Chem.*, 2015, **13**, 7584–7598.
- 11 A. S. Tatikolov, Polymethine Dyes as Spectral-Fluorescent Probes for Biomacromolecules, *J. Photochem. Photobiol., C*, 2012, **13**, 55–90.
- 12 J. L. Bricks, A. D. Kachkovskii, Y. L. Slominskii, A. O. Gerasov and S. V. Popov, Molecular Design of Near Infrared Polymethine Dyes: A Review, *Dyes Pigm.*, 2015, **121**, 238–255.
- 13 J. Fabian, H. Nakazumi and M. Matsuoka, Near-Infrared Absorbing Dyes, *Chem. Rev.*, 1992, **92**, 1197–1226.
- 14 A. Mishra, R. K. Behera, P. K. Behera, B. K. Mishra and G. P. Behera, Cyanines during the 1990's: A Review, *Chem. Rev.*, 2000, **100**, 1973–2011.
- 15 N. Tyutyulkov, J. Fabian, A. Melhorn, F. Dietz and A. Tadjer, *Polymethine Dyes: Structure and Properties*, St. Kliment Ohridski University Press, Bulgaria, 1991, pp. 1–250.
- 16 K. Jia, Y. Wan, A. Xia, S. Li., F. Gong and G. Yang, Characterization of Photoinduced Isomerization and Intersystem Crossing of the Cyanine Dye Cy3, *J. Phys. Chem. A*, 2007, **111**, 1593–1597.
- 17 Z. Huang, D. Ji, S. Wang, A. Xia, F. Koberling, M. Patting and R. Erdmann, Spectral Identification of Specific Photophysics of Cy5 by Means of Ensemble and Single Molecule Measurements, *J. Phys. Chem. A*, 2006, **110**, 45–50.
- 18 J. Widengren and P. Schwille, Characterization of Photoinduced Isomerization and Back-Isomerization of the Cyanine Dye Cy5 by Fluorescence Correlation Spectroscopy, *J. Phys. Chem. A*, 2000, **104**, 6416–6428.
- 19 J. A. Carr, D. Franke, J. R. Caram, C. F. Perkinson, M. Saif, V. Askoxylakis, M. Datta, D. Fukumura, M. G. Jain, M. G. Bawendi and O. T. Bruns, Shortwave Infrared

- Fluorescence Imaging with the Clinically Approved Near-Infrared Dye Indocyanine Green, *Proc. Natl. Acad. Sci. U. S. A.*, 2018, **115**, 4465–4470.
- 20 L. Štacková, E. Muchová, M. Russo, P. Slavíček, P. Štacko and P. Klán, Deciphering the Structure-Property Relations in Substituted Heptamethine Cyanines, *J. Org. Chem.*, 2020, **85**, 9776–9790.
- 21 Q. Zheng, S. Jockusch, Z. Zhou, R. B. Altman, J. D. Warren, N. J. Turro and S. C. Blanchard, On the Mechanisms of Cyanine Fluorophore Photostabilization, *J. Phys. Chem. Lett.*, 2012, **3**, 2200–2203.
- 22 S. S. Matikonda, G. Hammersley, N. Kumari, L. Grabenhorst, V. Glembockyte, P. Tinnefeld, J. Ivanić, M. Levitus and M. J. Schnermann, Impact of Cyanine Conformational Restraint in the Near-Infrared Range, *J. Org. Chem.*, 2020, **85**, 5907–5915.
- 23 A. M. Kolesnikov and F. A. Mikhailenko, The Conformations of Polymethine Dyes, *Russ. Chem. Rev.*, 1987, **56**, 275–287.
- 24 E. D. Cosco, J. R. Caram, O. T. Bruns, D. Franke, R. A. Day, E. P. Farr, M. G. Bawendi and E. M. Sletten, Flavylum Polymethine Fluorophores for Near- and Shortwave Infrared Imaging, *Angew. Chem., Int. Ed.*, 2017, **56**, 13126–13129.
- 25 E. D. Cosco, B. A. Arús, A. L. Spearman, T. L. Atallah, I. Lim, O. S. Leland, J. R. Caram, T. S. Bischof, O. T. Bruns and E. M. Sletten, Bright Chromenylum Polymethine Dyes Enable Fast, Four-Color *In Vivo* Imaging with Shortwave Infrared Detection, *J. Am. Chem. Soc.*, 2021, **143**, 6836–6846.
- 26 M. Kasha, Characterization of Electronic Transitions in Complex Molecules, *Discuss. Faraday Soc.*, 1950, **9**, 14–19.
- 27 C. Rullière, Laser Action and Photoisomerisation of 3,3'-Diethyl Oxadicarbocyanine iodide (DODCI): Influence of Temperature and Concentration, *Chem. Phys. Lett.*, 1976, **43**, 303–308.
- 28 F. Momicchioli, I. Baraldi and G. Berthier, Theoretical Study of Trans-Cis Photoisomerism in Polymethine Cyanines, *Chem. Phys.*, 1988, **123**, 103–122.
- 29 G. Ponterini and F. Momicchioli, Trans-Cis Photoisomerization Mechanisms of Carbocyanines: Experimental Check of Theoretical Models, *Chem. Phys.*, 1991, **151**, 111–126.
- 30 D. N. Dempster, T. Morrow, R. Rankin and G. F. Thompson, Photochemical Characteristics of Cyanine Dyes. Part 1. – 3,3'-Diethyloxadicarbocyanine Iodide and 3,3'-Diethylthiadibocyanine Iodide, *J. Chem. Soc., Faraday Trans. 2*, 1972, **68**, 1479–1496.
- 31 V. A. Kuzmin and A. P. Darmanyan, Study of Sterically Hindered Short-Lived Isomers of Polymethine Dyes by Laser Photolysis, *Chem. Phys. Lett.*, 1978, **54**, 159–163.
- 32 J.-P. Fouassier, D.-J. Loughnot and J. Faure, Transient Absorption in a Polymethine Laser Dye, *Chem. Phys. Lett.*, 1975, **35**, 189–194.
- 33 J.-P. Fouassier, D.-J. Loughnot and J. Faure, Étude Photo-physique D'une Série de Cyanines. I. – Processus D'évolution des États Excités, *J. Chem. Phys.*, 1977, **74**, 23–31.
- 34 J.-P. Fouassier, D.-J. Loughnot and J. Faure, Photoisomerization Processes in the IR-140 Laser Dye, *Opt. Commun.*, 1977, **23**, 393–397.
- 35 D. J. Loughnot, P. Brunero, J.-P. Fouassier and J. Faure, Etude Physicochimique d'Une Série de Cyanines. Partie IV: Rigidification, Photoisomerization et Effet Laser, *J. Chem. Phys.*, 1982, **79**, 343–349.
- 36 B. Kopainsky, P. Qiu and W. Kaiser, Lifetime, Photostability, and Chemical Structure of IR Heptamethine Cyanine Dyes Absorbing Beyond 1  $\mu\text{m}$ , *Appl. Phys. B*, 1982, **29**, 15–18.
- 37 W. Kranitzky, B. Kopainsky and W. Kaiser, A New Infrared Laser Dye of Superior Photostability Tunable to 1.24  $\mu\text{m}$  with Picosecond Excitation, *Opt. Commun.*, 1980, **36**, 149–152.
- 38 A. Sanchez-Galvez, P. Hunt, M. A. Robb, M. Olivucci, T. Vreven and H. B. Schlegel, Ultrafast Radiationless Deactivation of Organic Dyes: Evidence for a Two-State Two-Mode Pathway in Polymethine Cyanines, *J. Am. Chem. Soc.*, 2000, **122**, 2911–2924.
- 39 P. A. Hunt and M. A. Robb, Systematic Control of Photochemistry: The Dynamics of Photoisomerization of a Model Cyanine Dye, *J. Am. Chem. Soc.*, 2005, **127**, 5720–5726.
- 40 X. R. Zhu and J. M. Harris, Studies of Excited-State Absorption and Photoisomerization of Cyanine Dyes by Using Laser-Induced Anharmonic Thermal Gratings, *Chem. Phys.*, 1990, **142**, 301–309.
- 41 J. C. Mialocq, P. Goujon and M. Arvis, Etude par Spectroscopie Picoseconde et par Photolyse Eclair Conventionnelle de Polymethine-Cyanines, *J. Chem. Phys.*, 1979, **76**, 1067–1075.
- 42 C. Carre, C. Reichardt and D. J. Loughnot, Étude Physicochimique d'Une Série de Cyanines: – Partie VII: Rendement en état Triplet et Photosensibilisation de l'oxygène Singulet, *J. Chem. Phys.*, 1987, **84**, 575–585.
- 43 F. Köhn, J. Hofkens, R. Gronheid, M. Van der Auweraer and F. C. De Schryver, Parameters Influencing the On- and Off-Times in the Fluorescence Intensity Traces of Single Cyanine Dye Molecules, *J. Phys. Chem. A*, 2002, **106**, 4808–4814.
- 44 A. K. Chibisov, G. V. Zakharova and H. Görner, Effects of Substituents in the Polymethine Chain on the Photoprocesses in Indodicarbocyanine Dyes, *J. Chem. Soc., Faraday Trans.*, 1996, **92**, 4917–4925.
- 45 H. Gratz, A. Penzkofer, C. Abels, R.-M. Szeimies, M. Landthaler and W. Bäuml, Photo-Isomerisation, Triplet Formation, and Photo-Degradation Dynamics of Indocyanine Green Solutions, *J. Photochem. Photobiol., A*, 1999, **128**, 101–109.
- 46 A. T. Eske and K. R. Naqvi, Viscosity Dependence of the Fluorescence Lifetimes of Cryptocyanine, Pinacyanol and DDI, *Chem. Phys. Lett.*, 1979, **63**, 128–132.
- 47 A. K. Chibisov, G. V. Zakharova, H. Görner, Y. A. Sogulyaev, I. L. Mushkalo and A. I. Tolmachev, Photorelaxation Processes in Covalently Linked Indocarbocyanine and Thiocarbocyanine Dyes, *J. Phys. Chem.*, 1995, **99**, 886–893.
- 48 P. F. Aramendía, R. M. Negri and E. S. Román, Temperature Dependence of Fluorescence and Photoisomerization in Symmetric Carbocyanines. Influence of Medium Viscosity and Molecular Structure, *J. Phys. Chem.*, 1994, **98**, 3165–3173.
- 49 R. Engleman and J. Jortner, The Energy Gap Law for Radiationless Transitions in Large Molecules, *Mol. Phys.*, 1980, **18**, 145–164.

- 50 W. Siebrand and D. F. Williams, Radiationless Transitions in Polyatomic Molecules. III. Anharmonicity, Isotope Effects, and Singlet-to-Ground-State Transitions in Aromatic Hydrocarbons, *J. Chem. Phys.*, 1968, **49**, 1860–1871.
- 51 U. Dinur and B. Scharf, Radiationless Transitions in Linear Polyenes, *J. Chem. Phys.*, 1983, **79**, 2600–2608.
- 52 V. Chynwat and H. A. Frank, The Application of the Energy Gap Law to the  $S_1$  Energies and Dynamics of Carotenoids, *Chem. Phys.*, 1995, **194**, 237–244.
- 53 M. Mimuro, S. Seiji Akimoto, S. Shinichi Takaichi and I. Yamazaki, Effect of Molecular Structures and Solvents on the Excited State Dynamics of the  $S_2$  State of Carotenoids Analyzed by the Femtosecond Up-Conversion Method, *J. Am. Chem. Soc.*, 1997, **119**, 1452–1453.
- 54 H. A. Frank, V. Chynwat, R. Z. B. Desamero, R. Farhoosh, J. Erickson and J. Bautista, On the Photophysics and Photochemical Properties of Carotenoids and their Role as Light-Harvesting Pigments in Photosynthesis, *Pure Appl. Chem.*, 1997, **69**, 2117–2124.
- 55 G. Orlandi, F. Zerbetto and M. Z. Zgierski, Theoretical Analysis of Spectra of Short Polyenes, *Chem. Rev.*, 1991, **91**, 867–891.
- 56 N. J. Turro, V. Ramamurthy and J. C. Scaiano, *Principles of Molecular Photochemistry. An Introduction*, University Science Books, 2009, pp. 1–1084.
- 57 Y.-C. Wei, K.-H. Kuo, Y. Chi and P.-T. Chou, Efficient Near-Infrared Luminescence of Self-Assembled Platinum(II) Complexes: From Fundamentals to Applications, *Acc. Chem. Res.*, 2023, **56**, 689–699.
- 58 W. Siebrand, Radiationless Transitions in Polyatomic Molecules. I. Calculation of Franck–Condon Factors, *J. Chem. Phys.*, 1967, **46**, 440–447.
- 59 W. Siebrand, Radiationless Transitions in Polyatomic Molecules. II. Triplet-Ground-State Transitions in Aromatic Hydrocarbons, *J. Chem. Phys.*, 1967, **47**, 2411–2422.
- 60 H. C. Friedman, E. D. Cosco, T. L. Atallah, S. Jia, E. M. Sletten and J. R. Caram, Establishing Design Principles for Emissive Organic SWIR Chromophores from Energy Gap Laws, *Chem*, 2021, **7**, 3359–3376.
- 61 E. S. Medvedev and V. I. Osherov, *Radiationless Transitions in Polyatomic Molecules*, Springer-Verlag, Berlin Heidelberg, 1995, p. 88.
- 62 H. Mustroph and A. Towns, Fine Structure in Electronic Spectra of Cyanine Dyes: Are Sub-Bands Largely Determined by a Dominant Vibration or a Collection of Singly Excited Vibrations?, *ChemPhysChem*, 2018, **19**, 1016–1023.
- 63 G. Angulo, G. Grampp and A. Rosspeintner, Recalling the Appropriate Representation of Electronic Spectra, *Spectrochim. Acta, Part A*, 2006, **65**, 727–731.
- 64 V. A. Gilbert and J. Baggott, *Essentials of Molecular Photochemistry*, Blackwell Scientific, Oxford, 1991, pp. 1–538.
- 65 S. J. Strickler and R. A. Berg, Relationship between Absorption Intensity and Fluorescence Lifetime of Molecules, *J. Chem. Phys.*, 1962, **37**, 814–822.
- 66 J. E. Saunders, C. Sanders, H. Chen and H.-P. Loock, Refractive Indices of Common Solvents and Solutions at 1550 nm, *Appl. Opt.*, 2016, **55**, 947–953.
- 67 X. Li, C. Wang, L. Ma and L. Liu, Ellipsometry-Transmission Measurement of the Complex Refractive Indices for a Series of Organic Solvents in the 200–1700 nm Spectral Range, *Infrared Phys. Technol.*, 2022, **125**, 104313.
- 68 C. H. Brito Cruz, J. P. Gordon, P. C. Becker, R. L. Fork and C. V. Shank, Dynamics of Spectral Hole Burning, *IEEE J. Quantum. Electron.*, 1988, **24**, 261–265.
- 69 B. Dietzek, A. Yartsev and A. N. Tarnovsky, Watching Ultrafast Barrierless Excited-State Isomerization of Pseudocyanine in Real Time, *J. Phys. Chem. B*, 2007, **111**, 4520–4526.
- 70 S. A. Kovalenko, N. P. Ernsting and J. Ruthmann, Femtosecond Hole-Burning Spectroscopy of the Dye DCM in Solution: the Transition from the Locally Excited to a Charge-Transfer State, *Chem. Phys. Lett.*, 1996, **258**, 445–454.
- 71 S. A. Kovalenko, J. Ruthmann and N. P. Ernsting, Femtosecond Hole-Burning Spectroscopy with Stimulated Emission Pumping and Supercontinuum Probing, *J. Chem. Phys.*, 1998, **109**, 1894–1900.
- 72 C. Schweitzer and R. Schmidt, Physical Mechanisms of Generation and Deactivation of Singlet Oxygen, *Chem. Rev.*, 2003, **103**, 1685–1757.
- 73 S. L. Murov, I. Carmichael and G. L. Hug, *Handbook of Photochemistry*, Marcel Dekker, 1993, p. 290.
- 74 L. A. Shvedova, A. S. Tatikolov, S. M. Makin, N. N. Romanov and V. A. Kuzmin, Flash Photolysis of Tricarbocyanine Dyes, *Russ. Chem. Bull.*, 1979, **28**, 696–701.
- 75 A. N. Tarnovsky, T. K. Razumova, E. P. Shchelkina and T. V. Veselova, Photophysical, Photochemical, and Lasing Characteristics of Symmetric and Asymmetric Di- and Tricarbocyanine Dyes, *Opt. Spectrosc.*, 1993, **74**, 65–78 [*Opt. Spektrosk. (USSR)*, 1993, **74**, 107–129].
- 76 T. K. Razumova and A. N. Tarnovsky, Isomerization Processes in the Ground and First Excited States of 1-1'-Diethyl-2,2'-Dicarbocyanine Iodide (DDI), *Opt. Spectrosc.*, 1995, **78**, 56–63 [*Opt. Spektrosk. (USSR)*, 1995, **78**, 65–72].
- 77 J. S. Baskin, H.-Z. Yu and A. H. Zewail, Ultrafast Dynamics of Porphyrins in the Condensed Phase: I. Free Base Tetraphenylporphyrin, *J. Phys. Chem. A*, 2002, **42**, 9837–9844.
- 78 S. A. Kovalenko, R. Schanz, H. Hennig and N. P. Ernsting, Cooling Dynamics of an Optically Excited Molecular Probe in Solution from Femtosecond Broadband Transient Absorption Spectroscopy, *J. Chem. Phys.*, 2001, **115**, 3256–3273.
- 79 M. L. Horng, J. A. Gardecki, A. Papazyan and M. Maroncelli, Subpicosecond Measurements of Polar Solvation Dynamics: Coumarin 153 Revisited, *J. Phys. Chem.*, 1995, **99**, 17311–17337.
- 80 T. Elsaesser and W. Kaiser, Vibrational and Vibronic Relaxation of Large Polyatomic Molecules in Liquids, *Annu. Rev. Phys. Chem.*, 1991, **42**, 83–107.
- 81 E. L. Sibert III, S. G. Ramesh and T. S. Gulmen, Vibrational Relaxation of OH and CH Fundamentals of Polar and Nonpolar Molecules in the Condensed Phase, *J. Phys. Chem. A*, 2008, **112**, 11291–11305.
- 82 D. J. D. Miller, Vibrational Energy Relaxation and Structural Dynamics of Heme Proteins, *Annu. Rev. Phys. Chem.*, 1991, **42**, 581–614.

- 83 R. I. Personov, Site Selection Spectroscopy of Complex Molecules in Solutions and its Applications, in *Spectroscopy and Excitation Dynamics of Condensed Molecular Systems*, ed. V. M. Agranovich and R. M. Hochstrasser, 1983, ch. 10, pp. 555–619.
- 84 H. Murakami, S. Kinoshita, Y. Hirata, T. Okada and N. Mataga, Transient Hole-Burning and Time-Resolved Fluorescence Spectra of Dye Molecules in Solution: Evidence for Ground-state Relaxation and Hole-filling Effect, *J. Chem. Phys.*, 1992, **97**, 7881–7888.
- 85 S. Kinoshita, H. Itoh, H. Murakami, H. Miyasaka, T. Okada and N. Mataga, Solvent Relaxation Effect on Transient Hole-Burning Spectra of Organic Dyes, *Chem. Phys. Lett.*, 1990, **166**, 123–127.
- 86 S. Kinoshita, Theory of Transient Hole-burning Spectrum of Molecules in Solution, *J. Chem. Phys.*, 1989, **91**, 5175–5183.
- 87 K. Nishiyama and T. Okada, Relaxation of Inhomogeneous Spectral Band Width of Dye Molecules in Polar Solvents Studied by Time-Resolved Hole and Fluorescence Spectroscopy, *J. Phys. Chem. A*, 1997, **101**, 5729–5735.
- 88 K. Nishiyama and T. Okada, Relaxation Dynamics of Inhomogeneous Spectral Width in Binary Solvents Studied by Transient Hole-Burning Spectroscopy, *J. Phys. Chem. A*, 1998, **102**, 9729–9733.
- 89 H. Shirota and E. W. Castner Jr., Molecular Dynamics and Interactions of Aqueous and Dichloromethane Solutions of Polyvinylpyrrolidone, *J. Chem. Phys.*, 2006, **125**, 034904.
- 90 B. Dietzek, B. Brüggemann, P. Persson and A. Yartsev, On the Excited-state Multi-Dimensionality in Cyanines, *Chem. Phys. Lett.*, 2008, **455**, 13–19.
- 91 I. Renge, Mechanisms of Solvent Shifts, Pressure Shifts, and Inhomogeneous Broadening of the Optical Spectra of Dyes in Liquids and Low-Temperature Glasses, *J. Phys. Chem. A*, 2000, **104**, 7452–7463.
- 92 I. Renge and U. P. Wild, Solvent, Temperature, and Excitonic Effects in the Optical Spectra of Pseudoisocyanine Monomer and J-Aggregates, *J. Phys. Chem. A*, 1997, **101**, 7977–7988.
- 93 B. Dietzek, A. N. Tarnovsky and A. Yartsev, Visualizing Overdamped Wavepacket Motion: Excited-state Isomerization of Pseudocyanine in Viscous Solvents, *Chem. Phys.*, 2009, **357**, 54–62.
- 94 C. A. Guarín, J. P. Villabona-Monsalve, R. López-Arteaga and J. Peon, Dynamics of the Higher Lying Excited States of Cyanine Dyes. An Ultrafast Fluorescence Study, *J. Phys. Chem. B*, 2013, **117**, 7352–7362.
- 95 I. Martini and G. V. Hartland, Ultrafast Investigation of Vibrational Relaxation in the S<sub>1</sub> Electronic State of HITC, *J. Phys. Chem.*, 1996, **100**, 19764–19770.
- 96 I. Martini and G. V. Hartland, Relaxation Dynamics in the First Excited Singlet State of a Cyanine Dye: HITC, *Chem. Phys. Lett.*, 1996, **258**, 180–186.
- 97 C. T. Middleton, B. Cohen and B. Kohler, Solvent and Solvent Isotope Effects on the Vibrational Cooling Dynamics of a DNA Base Derivative, *J. Phys. Chem. A*, 2007, **111**, 10460–10467.
- 98 T.-S. Yang, M.-S. Chang, R. Chang, M. Hayashi, S. H. Lin, P. Vöhringer, W. Dietz and N. F. Scherer, Femtosecond Pump-probe Study of Molecular Vibronic Structures and Dynamics of a Cyanine Dye in Solution, *J. Chem. Phys.*, 1999, **110**, 12070–12081.
- 99 D. K. Das, K. Makhil and D. Goswami, Observing Ground State Vibrational Coherence and Excited State Relaxation Dynamics of a Cyanine Dye in Pure Solvents, *Phys. Chem. Chem. Phys.*, 2018, **20**, 13400–13411.
- 100 J. M. Jean and G. R. Fleming, Competition between Energy and Phase Relaxation in Electronic Curve Crossing Processes, *J. Chem. Phys.*, 1995, **103**, 2092–2101.
- 101 T. Fuji, H. J. Ong and T. Kobayashi, Real-time Observation of Vibrational Coherence Persisting after Internal Conversion and Vibrational Relaxation in Cyanine Dye Molecules, *Chem. Phys. Lett.*, 2003, **380**, 135–140.
- 102 F. W. Wise, M. J. Rosker and C. L. Tang, Oscillatory Femtosecond Relaxation of Photoexcited Organic Molecules, *J. Chem. Phys.*, 1987, **86**, 2827–2832.
- 103 A. Yu, C. A. Tolbert, D. A. Farrow and D. M. Jonas, Solvatochromism and Solvation Dynamics of Structurally Related Cyanine Dyes, *J. Phys. Chem. A*, 2002, **106**, 9407–9419.
- 104 J.-C. Gummy, O. Nicolet and E. Vauthey, Investigation of the Solvation Dynamics of an Organic Dye in Polar Solvents using the Femtosecond Transient Grating Technique, *J. Phys. Chem. A*, 1999, **103**, 10737–10743.
- 105 M. M. Bishop, J. D. Roscioli, S. Ghosh, J. J. Mueller, N. C. Shepherd and W. F. Beck, Vibrationally Coherent Preparation of the Transition State for Photoisomerization of the Cyanine Dye Cy5 in Water, *J. Phys. Chem. B*, 2015, **119**, 6905–6915.
- 106 S. M. Hart, J. L. Banal, M. Bathe and G. S. Schlau-Cohen, Identification of Nonradiative Decay Pathways in Cy3, *J. Phys. Chem. Lett.*, 2020, **11**, 5000–5007.
- 107 Z. Wei, T. Nakamura, S. Takeuchi and T. Tahara, Tracking of the Nuclear Wavepacket Motion in Cyanine Photoisomerization by Ultrafast Pump-Dump-Probe Spectroscopy, *J. Am. Chem. Soc.*, 2011, **133**, 8205–8210.
- 108 C. J. Bardeen, Q. Wang and C. V. Shank, Femtosecond Chirped Pulse Excitation of Vibrational Wave Packets in LD690 and Bacteriorhodopsin, *J. Phys. Chem. A*, 1998, **102**, 2759–2766.
- 109 T. Teramoto and T. Kobayashi, Multiple Mode Coupling in Cy3 Molecules by Impulsive Coherent Vibrational Spectroscopy Using a Few-Cycle Laser Pulse, *Phys. Chem. Chem. Phys.*, 2010, **12**, 13515–13518.
- 110 B. Dietzek, T. Pascher and A. Yartsev, Tracking Ultrafast Excited-State Bond-Twisting Motion in Solution Close to the Franck-Condon Point, *J. Phys. Chem. B*, 2007, **111**, 6034–6041.
- 111 B. Dietzek, B. Brüggemann, T. Pascher and A. Yartsev, Pump-Shaped Dump Optimal Control Reveals the Nuclear Reaction Pathway of Isomerization of a Photoexcited Cyanine Dye, *J. Am. Chem. Soc.*, 2007, **129**, 13014–13021.
- 112 B. Dietzek, B. Brüggemann, T. Pascher and A. Yartsev, Mechanisms of Molecular Response in the Optimal

- Control of Photoisomerization, *Phys. Rev. Lett.*, 2006, **97**, 258301(4).
- 113 D. H. Waldeck, Photoisomerization Dynamics of Stilbenes, *Chem. Rev.*, 1991, **91**, 415–436.
- 114 G. R. Fleming, *Chemical Applications of Ultrafast Spectroscopy*, Oxford University Press, 1986, p. 186.
- 115 P. Hänggi, P. Talkner and M. Borkovec, Reaction- Rate Theory: Fifty Years after Kramers, *Rev. Mod. Phys.*, 1990, **62**, 251–341.
- 116 S. P. Velsko, D. H. Waldeck and G. R. Fleming, Breakdown of Kramers Theory Description of Photochemical Isomerization and the Possible Involvement of Frequency Dependent Friction, *J. Chem. Phys.*, 1983, **78**, 249–258.
- 117 K. Hara and S. Akimoto, High-Pressure Study of the Viscosity Effect on the Ground-State Isomerization of 3,3'-Diethyloxadicarbocyanine Iodide (DODCI), *J. Phys. Chem.*, 1991, **95**, 5811–5814.
- 118 V. Sundström and T. Gillbro, Effects of Solvent on TMP Photophysics. Transition from no Barrier to Barrier Case, Induced by Solvent Properties, *J. Chem. Phys.*, 1984, **81**, 3463–3474.
- 119 E. Åkesson, V. Sundström and T. Gillbro, Solvent-Dependent Barrier Heights of Excited-State Photoisomerization Reactions, *Chem. Phys. Lett.*, 1985, **121**, 513–522.
- 120 G. Ponterini and M. Caselli, Photoisomerization Dynamics of 3,3'-Diethyl Oxacarbocyanine. Intramolecular and Solvent Viscosity Effects, *Ber. Bunsenges. Physik. Chem.*, 1992, **96**, 564–573.
- 121 J. Korppi-Tommola, A. Hakkarainen, T. Hukka and J. Subbi, An Isomerization Reaction of a Cyanine Dye in *n*-Alcohols: Microscopic Friction and an Excited-State Barrier Crossing, *J. Phys. Chem. A*, 1991, **95**, 8482–8491.
- 122 N. Hirai and H. Henry Eyring, Bulk Viscosities of Liquids, *J. Appl. Phys.*, 1958, **29**, 810–816.
- 123 D. R. Lide, *RC Handbook of Chemistry and Physics*, CRC Press LLC, Boca Raton, 90th edn, 1990, pp. 6–209.
- 124 H. C. Friedman, E. D. Cosco, T. L. Atallah, S. Jia, E. M. Sletten and J. R. Caram, Establishing Design Principles for Emissive Organic SWIR Chromophores from Energy Gap Laws, *Cell*, 2021, **7**, 3359–3376.
- 125 E. Åkesson, A. Hakkarainen, E. Laitinen, V. Helenius, T. Gillbro, J. Korppi-Tommola and V. Sundström, Analysis of Microviscosity and Reaction Coordinate Concepts in Isomerization Dynamics Described by Kramers' Theory, *J. Chem. Phys.*, 1991, **95**, 6508–6523.
- 126 S. Murphy and G. B. Schuster, Electronic Relaxation in a Series of Cyanine Dyes: Evidence for Electronic and Steric Control of the Rotational Rate, *J. Phys. Chem.*, 1995, **99**, 8516–8518.
- 127 D. Bingemann and N. P. Ernsting, Femtosecond Solvation Dynamics Determining the Band Shape of Stimulated Emission from a Polar Styryl Dye, *J. Chem. Phys.*, 1995, **102**, 2691–2700.
- 128 S. H. Ashworth, T. Hasche, M. Woerner, E. Riedle and T. Elsaesser, Vibronic Excitations of Large Molecules in Solution Studied by Two-Color Pump-Probe Experiments on the 20 fs Time Scale, *J. Chem. Phys.*, 1996, **104**, 5761–5769.
- 129 Y. H. Meyer, M. Pittman and P. Plaza, Transient Absorption of Symmetrical Carbocyanines, *J. Photochem. Photobiol., A*, 1998, **114**, 1–21.
- 130 S. A. Kovalenko, J. Ruthmann and N. P. Ernsting, Ultrafast Stokes Shift and Excited-State Transient Absorption of Coumarin 153 in Solution, *Chem. Phys. Lett.*, 1997, **271**, 40–50.
- 131 A. Müller, J. Schulz-Hennig and H. Tashiro, Excited State Absorption of 1,3,3,1',3',3'-Hexamethylindotricarbocyanine Iodide: A Quantitative Study by Ultrafast Absorption Spectroscopy, *Appl. Phys.*, 1977, **12**, 333–339.
- 132 R. S. Lepkowitz, O. V. Przhonska, J. M. Hales, D. J. Hagan, E. W. Van Stryland, M. V. Bondar, Y. L. Slominsky and A. D. Kachkovski, Excited-State Absorption Dynamics in Polymethine Dyes Detected by Polarization-Resolved Pump-Probe Measurements, *Chem. Phys.*, 2003, **286**, 277–291.
- 133 E. Sandberg, J. Piguet, U. Kostiv, G. Baryshnikov, H. Liu and J. Widengren, Photoisomerization of Heptamethine Cyanine Dyes Results in Red-Emissive Species: Implications for Near-IR, Single-Molecule, and Super-Resolution Fluorescence Spectroscopy and Imaging, *J. Phys. Chem. B*, 2023, **127**, 3208–3222.
- 134 E. Sandberg, J. Piguet, H. Liu and J. Widengren, Combined Fluorescence Fluctuation and Spectrofluorometric Measurements Reveal a Red-Shifted, Near-IR Emissive Photoisomerized Form of Cyanine 5, *Int. J. Mol. Sci.*, 2023, **24**, 1990.
- 135 K. Furuta, M. Fuyuki and A. Wada, Multiphoton Reaction of DTTCI Observed by Femtosecond Pump-probe and Two-pulse Correlation Measurements, *Chem. Phys.*, 2013, **418**, 42–46.
- 136 M. Fuyuki, K. Furuta and A. Wada, New Photoisomerization Path of Indocyanine Green in Condensed Phase Investigated by Two-Pump Excitation, *Chem. Phys. Lett.*, 2010, **499**, 121–125.
- 137 R. W. Redmond, I. E. Kochevar, M. Kreig, G. Smith and W. G. J. McGimpsey, Excited State Relaxation in Cyanine Dyes: A Remarkably Efficient Reverse Intersystem Crossing from Upper Triplet Levels, *J. Phys. Chem. A*, 1997, **101**, 2773–2777.
- 138 E. M. C. Hillman, Optical Brain Imaging *In Vivo*: Techniques and Applications from Animal to Man, *J. Biomed. Opt.*, 2007, **12**, 1–28.
- 139 Y. Yagci, S. Jockusch and N. J. Turro, Mechanism of Photoinduced Step Polymerization of Thiophene by Onium Salts: Reactions of Phenyliodonium and Diphenylsulfonium Radical Cations with Thiophene, *Macromolecules*, 2007, **40**, 4481–4485.
- 140 S. K. Pal, A. S. Mereshchenko, E. V. Butaeva, P. Z. El-Khoury and A. N. Tarnovsky, Global Sampling of the Photochemical Reaction paths of Bromoform by Ultrafast Deep-UV through Near-IR Transient Absorption and ab initio Multi-configurational Calculations, *J. Chem. Phys.*, 2013, **138**, 124501.

- 141 F. T. Gameda, V. Vorobyev and A. N. Tarnovsky, Ultrafast Solution-Phase Photophysical and Photochemical Dynamics of Hexaiodobismuthate(III), the Heart of Bismuth Halide Perovskite Solar Cells, *J. Phys. Chem. B*, 2022, **126**, 1254–1267.
- 142 S. A. Kovalenko, A. L. Dobryakov, J. Ruthmann and N. P. Ernsting, Femtosecond Spectroscopy of Condensed Phases with Chirped Supercontinuum Probing, *Phys. Rev. A: At., Mol., Opt. Phys.*, 1999, **59**, 2369–2384.
- 143 K. Ekvall, P. van der Meulen, C. Dhollande, L.-E. Berg, S. Pommeret, R. Naskreski and J.-C. Mialocq, Cross Phase Modulation Artifact in Liquid Phase Transient Absorption Spectroscopy, *J. Appl. Phys.*, 2000, **87**, 2340–2352.
- 144 S. A. Kovalenko, N. P. Ernsting and J. Ruthmann, Femtosecond Hole-Burning Spectroscopy of the Dye DCM in Solution: the Transition from the Locally Excited to a Charge-Transfer State, *Chem. Phys. Lett.*, 1996, **258**, 445–454.
- 145 H. J. Marrinan and N. Sheppard, Relative Intensities of the Raman Lines of Carbon Tetrachloride, Chloroform, and Methylene Chloride, *J. Opt. Soc. Am.*, 1954, **44**, 815–819.